Small Satellite Deployment Mechanisms

S. Pellegrino, S. Kukathasan, G. Tibert
and A. Watt

CUED/D-STRUCT/TR190

The work presented in this report was partially supported by research contract no. CU009-0000004842 between the Defence Evaluation Research Agency and the University of Cambridge, on behalf of the British National Space Centre. Technical monitor: Tim Reynolds.

Release date: 9 November, 2000.

Summary

This report presents a series of studies of deployable structures for future small satellite missions. A spacecraft bus with dimensions of $0.6 \times 0.6 \times 0.8$ m^3 is assumed and the deployable structures are required to fit alongside the bus, in an envelope not exceeding $0.6 \times 0.2 \times 0.8$ m^3.

Three types of requirements are considered, as follows: booms for space based GPS applications; 1.5–2 kW solar arrays; X-band (9.65 GHz) SAR's requiring either a 3 m diameter parabolic reflector or a 5×1.5 m^2 planar array.

This report presents three novel deployable structures that have been developed to meet these requirements. These structures make use of very recent developments in terms of packaging concepts and self-locking spring hinges, which make it possible to design low-cost structures with low mass.

Two schemes for 1.5 kW solar arrays are proposed. The first envisages a 2.4×3.0 m^2 flat array consisting of 15, 0.5 mm thick panels covered with photovoltaic cells. An outline design of this structure, having a fundamental natural frequency of 0.4 Hz and mass of 17.5 kg is developed. The second structure is a concentrator array of similar dimensions, where 10 of the panels are replaced with "cold mirror" panels. A design of this structure is developed, having a fundamental frequency of 0.6 Hz and a mass of 9 kg.

Next, a concept for a 3 m diameter $\approx$10 GHz parabolic reflector with focal-length-to-diameter ratio of 0.4 is presented. It is based on a tensegrity structure concept where the struts are collapsible and its estimated mass is 9 kg.

Finally, a "reflectarray" split SAR is presented consisting of two 2.4×1.6 m^2 structures that are separately deployed on either side of the spacecraft bus. An outline design of this structure is presented, having a total mass of around 31 kg and a fundamental natural frequency of 0.9 Hz.

Contents

List of Figures

Chapter 1

Introduction

This report presents a series of pilot studies that were carried in the Deployable Structures Laboratory during the period March–September 2000, in conjunction with DERA, on behalf of the British National Space Centre. In parallel with these studies, DERA formulated outline requirements for a range of deployable structures that could be used for future missions in DERA's STRV program, which currently uses a spacecraft bus with dimensions of $0.6 \times 0.6 \times 0.8$ m^3.

DERA's requirements can be divided into three categories, as follows: booms for space based GPS applications; 1.5–2 kW solar arrays; X-band (9.65 GHz) SAR requiring either a 3 m diameter parabolic reflector or a 5×1.5 m^2 planar array. All of these structures are subject to the same, very stringent constraints on the dimensions of the packaged envelope. These constraints were derived from the current launch configuration of the STRV platform, attached to the Ariane Structure for Auxiliary Payloads (ASAP) on the Ariane 5 launcher as shown in Figure 1.1.

On either side of the spacecraft bus there is an envelope 800 mm high by 200 mm deep (not shown in the figure) by 100 mm wide. It may be possible to extend some of these dimensions by negotiation with Arianespace but, since there is a *hard limit* of 891 mm on the height of the package, in this study it was assumed that no increase in the maximum height of the package will be allowed.

Because most of the existing deployable structures technologies were aimed at large spacecraft applications, new technology is required to meet the DERA requirements. Hence, various novel solutions for meeting the requirements were identified during the initial phase of the present study. These solutions were reviewed by DERA, following a progress meeting at Cambridge. A number of concepts were then selected for further investigation and were further developed

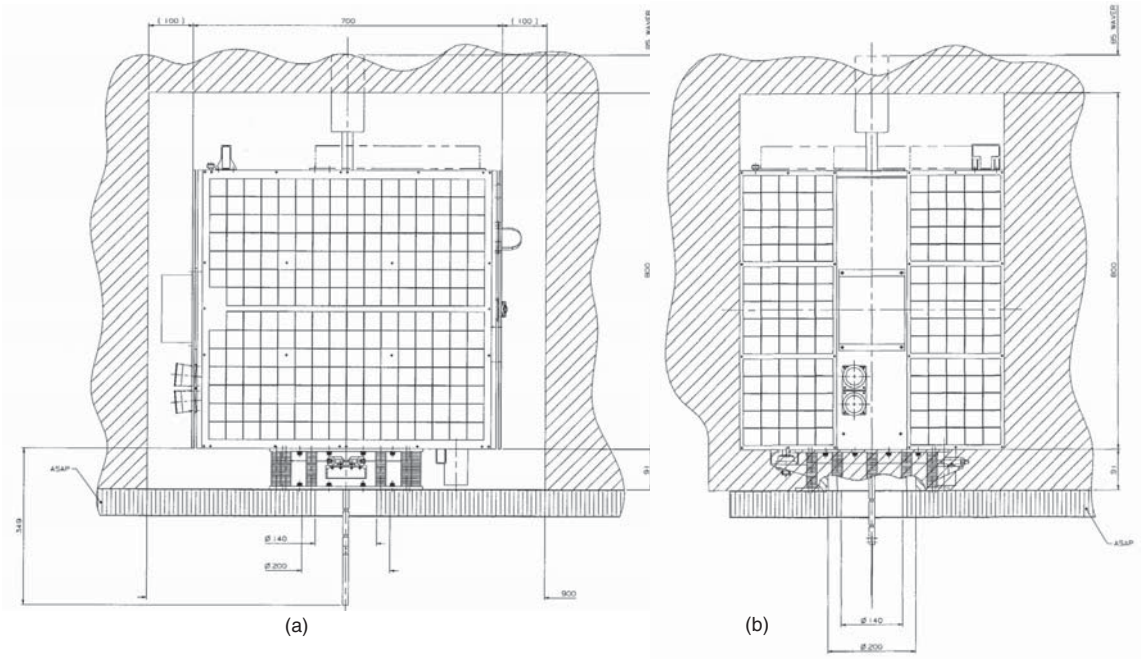

Figure 1.1: (a) Front and (b) side views of STRV on ASAP ring.

during the second phase of the study.

1.1 Aims and Scope of Report

This report presents three novel deployable structures that have been developed in response to DERA's requirements. These structures make use of very recent developments in terms of packaging concepts and self-locking spring hinges, which make it possible to design low-cost structures with low mass.

The feasibility of the structures that are proposed has been demonstrated by means of physical models and finite-element models, based on which preliminary designs were developed in order to obtain realistic mass estimates. During the study, a strong emphasis was placed on solutions that will require only spring-driven deployment, in order to keep to a minimum the number of actuators.

As with all pilot studies, this report should be seen as an initial step in the development of advanced deployable structures for small satellites. More detailed analysis and design, as well as the construction and testing of proper demonstrator hardware, will be required to further evaluate the proposed solutions.

1.2 Layout of Report

This report is divided into five chapters. Following this introduction, Chapter 2 identifies a range of solutions that could potentially meet DERA's requirements, and which were identified during the first phase of the study.

Chapter 3 further develops two schemes for 1.5 kW solar arrays. The first is a 2.4×3.0 m^2 flat array consisting of 15 panels covered with photovoltaic cells, with a fundamental natural frequency of 0.4 Hz and a mass of 17.5 kg. The second structure is a concentrator array of similar dimensions, with a fundamental frequency of 0.6 Hz and a mass of 9 kg.

Chapter 4 presents a scheme for a 3 m diameter $\approx$10 GHz parabolic reflector with focal-length-to-diameter ratio of 0.4. It is based on a tensegrity structure concept where the struts are made collapsible and its estimated mass is 9 kg.

Chapter 5 presents a reflectarray split SAR consisting of two 2.4×1.6 m^2 structures that are separately deployed on either side of the spacecraft bus. Each structure has a mass of around 15.5 kg and a fundamental natural frequency of 0.9 Hz.

Separate discussions of the concepts presented in Chapters 3–5 follow at the end of the relevant chapter.

Chapter 2

Review of Solution Schemes

2.1 GPS Booms

The main requirement is for a minimum of two and a maximum of three GPS sensors to be located at a distance d ranging between 1.2 and 3.2 m. This can be met with rigid carbon fibre booms with either one or two self-locking hinges. For example, the hinges could be the Tape-Spring Rolamite (TSR) hinges that have recently been developed in the Deployable Structures Laboratory, see Section 3.2.1.

Two-hinged booms would be required for a sensor separation of around 3 m. Depending on the selected boom length, they would be folded either on top of the bus or on a side. The absolute limit on the length of a rigid piece, including the hinges would be $\sqrt{0.6^2 + 0.8^2} = 1$ m if the booms are placed along the diagonals of the side panels. This is an already mature technology and it would be possible to begin designing the hardware required to meet a specified target performance without further development.

There is an alternative requirement for booms capable of delivering a separation $d = 20 - 30$ m. This is much more challenging and is likely to require the development of new technology.

The only mature technology that would be suitable is a Stainless Steel tubular boom of the bi-STEM type, see Figure 2.1. Each boom is contained within its own deployment cassette and is controlled by an electric motor.

A UK made Rolatube composite boom (Iqbal and Pellegrino, 2000) would require smaller deployment cassettes and may eliminate the need for electric motors.

DERA have specified a requirement of ± 5 mm for geometric stability; this is achievable for the shorter booms but is well beyond the capabilities of all open-section tubular booms mentioned above. DERA have indicated that software compensation for beam flexure and torsion could be

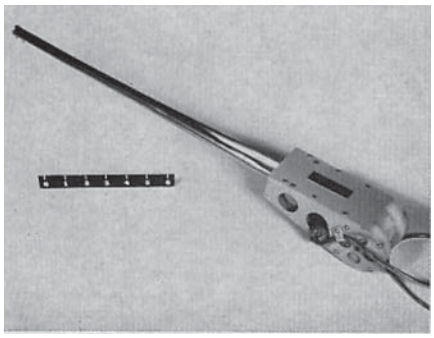

Figure 2.1: Bi-STEM boom.

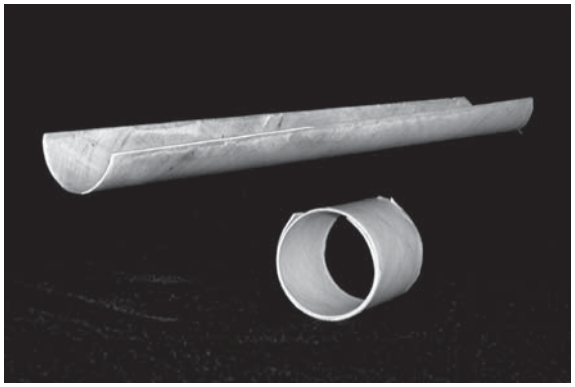

Figure 2.2: Rolatube boom.

provided; this is certainly worth considering for the longer booms.

Once the geometric stability requirements and loading conditions have been defined more clearly, the following options could be of interest.

- Add Velcro or high tack adhesive layers along the edges of a Rolatube.
- Consider the possibility of using inflatable booms. However, note that the mass of the make-up gas required will depend on the specified mission duration and orbit.
- Consider the possibility of using a tensegrity-type truss structure. The feasibility of this approach has been recently demonstrated by Pak (2000).

In conclusion, there exist several solutions that can meet either set of requirements. New technology will need to be developed if the longer booms are selected, unless the geometric stability requirements cannot be relaxed very significantly.

2.2 Solar Array

The requirement is for a 1.5–2 kW array; a preliminary estimate of its overall surface area can be obtained by assuming a design based on carbon-fibre reinforced Kapton covered with triple-junction cells flexible array. Reynolds (2000) provides the following data for flexible arrays, power = 213 W/m^2, mass =2.5 kg/m^2, and thickness =0.5 mm.[1] The corresponding array surface is 6.7–9 m^2 and the mass 14–19 kg, without the support structure. Four possible structural schemes are outlined below.

Scheme 1: Single Frame, Double Concertina Fold of Membrane

This scheme is shown in Figure 2.3. The frame folds transversally and then longitudinally into a 600 mm by 800 mm stack; this requires several straight folds in the membrane. Note that the axes of the hinges in each side of the frame are perpendicular to that side and all hinges are coplanar; the corners of the frame are rigid, i.e. there are no hinges. All hinges would be self-locking hinges, e.g. of the type shown in Figure 3.7.

Scheme 2: Fold-and-Roll-up Blanket with Deployable Boom

Figure 2.4 shows a scheme where the blanket supporting the cells is tensioned by two end bars, each with two articulations. The blanket is folded over twice, together with the end bars, before being rolled over a roller. The deployable backbone of this structure is a tubular

[1] Hence folding the membrane and cells with a fairly tight radius should be no problem.

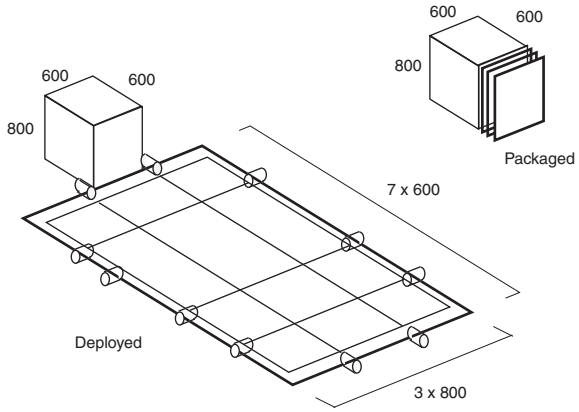

Figure 2.3: Double concertina fold scheme.

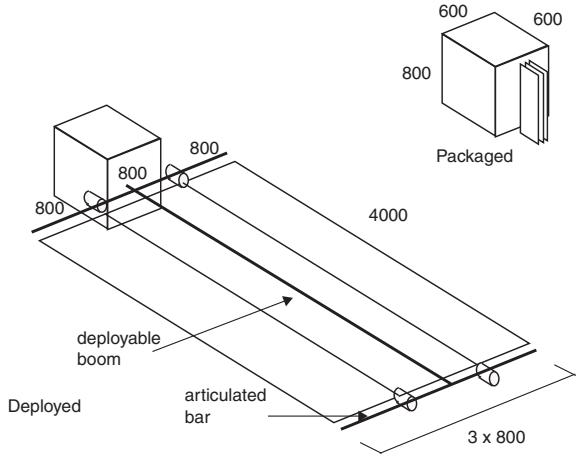

Figure 2.4: Double fold and roll-up solar array.

boom. This could be a Rolatube composite boom, in order to reduce the size of the deployment cassette. An ordinary bi-STEM (diameter around 30 mm and thickness of 0.2 mm or less) would be insufficiently stiff but a Rolatube could have much larger diameter and thickness. Lack of sufficient torsional stiffness could be a problem, hence some form of zippering of the open-section boom would be required.

As a possible variant, a concentrator array would be possible, with a trough configuration of the blanket.

Scheme 3: Two Foldable Frames

The concept shown in Figure 2.5 consists of a frame divided up into 800 mm long parts and connected by TSR hinges arranged in various directions. The frame folds as a bundle of ap-

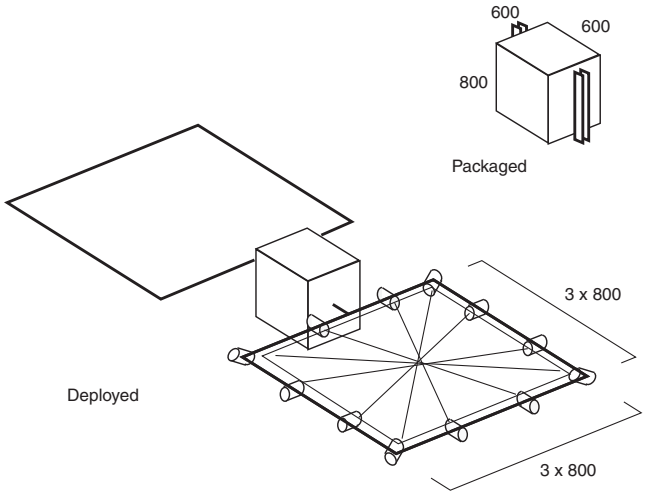

Figure 2.5: Solar arrays that fold into two bundles of bars.

proximately parallel bars and the blanket is packaged between the bars. A frame with seven hinges will have mobility of one, and hence would exhibit well-controlled deployment behaviour without the addition of any coupling devices. However, a much greater number of hinges is required to achieve the required packaging and so it is likely that some kinematic couplers, e.g. wires or rods, will need to be introduced. For the particular configuration shown in the figure there would be a limit of

$$2 \times (2.4 \times 2.4) = 11.5 \text{ m}^2$$

on the maximum total surface area.

Scheme 4: Two Foldable Plate Structures

Mr John Robertson has recently proposed an ingenious folding scheme for a structure consisting of rigid triangular plates. The plates are connected by hinges along the edges, and additional hinges are introduced along one set of diagonals, Figure 2.6. Given that the hinges can be as wide as the panels, there are several self-locking hinge designs that would be suitable as connections between the panels.

In this scheme higher efficiency rigid cells, capable of generating 300 Wm^2 (Reynolds, 2000), could be used; hence a smaller surface would be required. However, the folding scheme only works for squares forming a grid up to three by three, hence the maximum side length of the array would be 1.8 m; so two array wings would be required. There are, of course, simpler configurations of foldable structures consisting of square plates, but these alternatives would not allow all adjacent panels to be connected by hinges, and so would be less stiff.

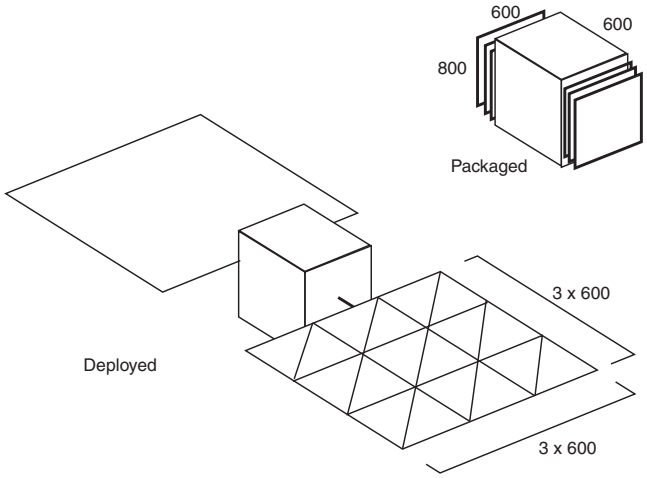

Figure 2.6: Solar arrays that fold into two stacks of plates.

2.3 Parabolic Reflector

What is needed is a reflector surface with accuracy better than 0.3 mm root-mean-square, but the packaging requirements are so stringent that none of the existing deployable reflector structures would be suitable. An inflatable antenna might be an option, but this approach has yet to be proven. The developments by Contraves (Switzerland) in the 1980's and more recently by L'Garde (USA) indicate that the low-cost, high structural efficiency promise of inflatable reflectors cannot be delivered in the near term.

An extension of the work by Pak (2000) is believed to be possible. It would combine the current state-of-the-art AstroMesh reflector with a deployable ring structure that can be collapsed to a very small size. The reflective surface is formed by a metallic mesh supported by a prestressed cable net, which is in turn supported by a cable and strut deployable ring. This approach appears to be able to meet the DERA requirement, but more work on this concept is needed before it can be properly assessed.

2.4 SAR Structure

The initial requirement was for a 5×1.5 m^2 SAR structure. The overall surface area is at the lower end of the range for the solar array, discussed in Section 2.2, but DERA estimate its mass to be around 3 kg/m^2, which is 50% higher than for the solar array.

Two different approaches are available. The more traditional scheme would be to mount the TR modules on rigid panels connected by hinges. The packaging requirements are basically the

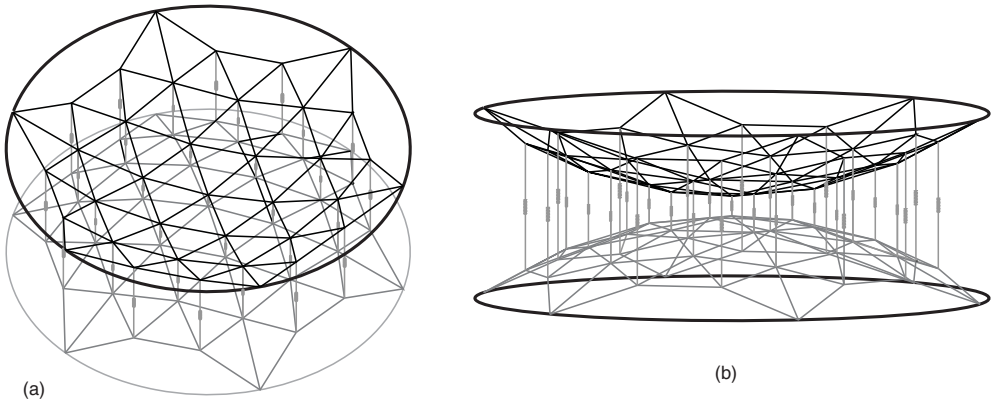

Figure 2.7: Deployable reflector concept consisting of two cable nets prestressed against one another and supported by a deployable ring; (a) perspective view and (b) side view).

same as in Section 2.2 and so the solutions discussed for the flat solar array are applicable.

Alternatively, various lighter weight solutions can be considered. For example, JPL have developed a lightweight SAR where three membranes covered with Copper printed circuits are rolled up together. The reflectarray envisaged by Reynolds (2000) would require only a single membrane. None of the solutions discussed in Section 2.2 would work for this type of membrane, as it would require the membrane to be folded and then rolled up. It is thought that this would damage the printed circuits, but further work on this issue is needed.

Following recent work in the Deployable Structures Laboratory (Pellegrino et al. 1999, Watt 2000), it was proposed that a solution for a rectangular frame with six TSR hinges that deploys a rolled-up membrane be taken further. Specifically, the following two solutions were identified.

Scheme 1: Single SAR Wing

The existing deployable frame has a ratio of about two to one; mounting three such frames in series gives the structure shown in Figure 2.8. Three separate rectangular membranes are rolled up, one on each frame. The width of this structure is determined by the length of the transverse elements, i.e. 0.8 m; its length is 4.8 m. This would provide a narrower surface than required.

Scheme 2: Split SAR

By arranging the rectangular frames sideways the width of the structure can be increased. Figure 2.9 shows a scheme offering a maximum width of 1.6 m, but obviously the deployment will become more complex to control as the number of frames is increased. Hence, it was thought that a length of around 5 m would be difficult to achieve in a single wing and so it is assumed

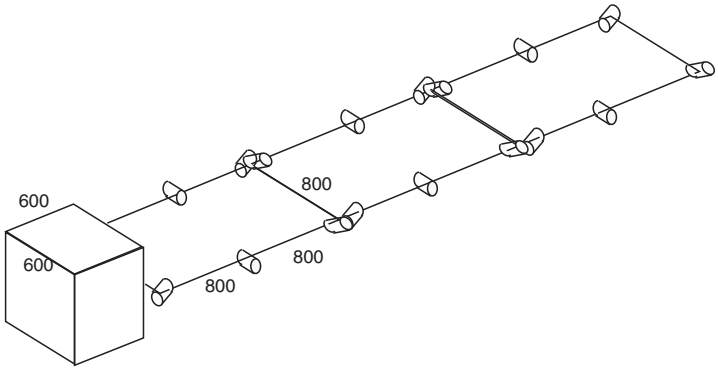

Figure 2.8: Concept for SAR structure, consisting of three foldable frames supporting roll-up blankets.

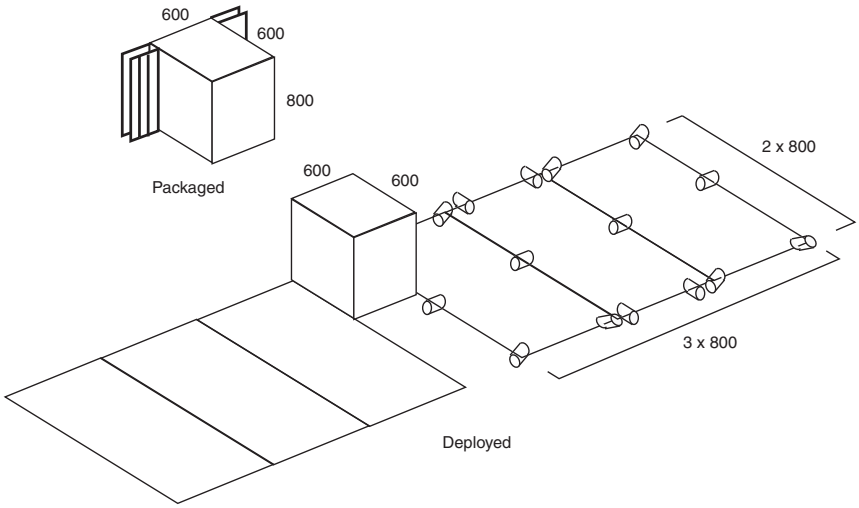

Figure 2.9: Interconnected foldable frames, each supporting a roll-up blanket.

that the SAR would in fact consist of two separate wings, according to the *displaced antenna option* considered by Reynolds (2000).

2.5 Selection of Concepts for Further Investigation

After a review of the solutions described above, jointly with DERA, it was decided to investigate further one structure for each application. The following concepts were selected.

- Solar array. The double-concertina fold scheme in Figure 2.3.
- Reflector. The only option that had been identified in the first phase of the study, namely

the structure shown in Figure 2.7.

- SAR. The interconnected frame solution in Figure 2.9.

Chapter 3

Solar Array Structures

Two different configurations of a flexible solar array capable of generating about 1.5 kW are considered. The first configuration, Figure 3.1(a), provides a *flat* arrangement of 15 thin panels, of size 0.6×0.8 m^2 covered with photovoltaic cells. The second configuration, Figure 3.1(b), provides 5 thin panels covered with photovoltaic cells, at the centre of a *trough* whose sides are formed by 10 panels acting as "cold mirror" reflective surfaces. In both configurations, structural stiffness and integrity are provided by a deployable edge frame consisting of rigid elements and TSR hinges. An almost square configuration of the array has been achieved by arranging the 0.8 m long members along the short side of the rectangle. An advantage of this configuration is that it reduces the length of the array and thus increases its fundamental natural frequency. However, the folded array has to be rotated 90° to fit alongside the bus, which increases the complexity of the attachment mechanism.

The panels covered with photovoltaic cells have a total thickness of 0.5 mm, which includes a carbon fibre/kapton membrane, the photovoltaic cells, and a glass cover; their mass is 2.1 kg/m^2. The reflector panels have a mass of 0.26 kg/m^2. It is envisaged that the panels will be fastened to a grid of cords prestressed against the frame. Further details can be found in Reynolds (2000).

3.1 Proposed Mechanism Concept

Both configurations of the solar array involve 15 rectangular panels which cannot themselves be easily folded; hence the proposed folding scheme assumes that the panels remain essentially undeformed.

The panels are connected by flexible hinges (e.g. consisting of strips of Kapton foil glued to one side of the panel). Hence, the most obvious folding scheme is to activate the two longitudinal

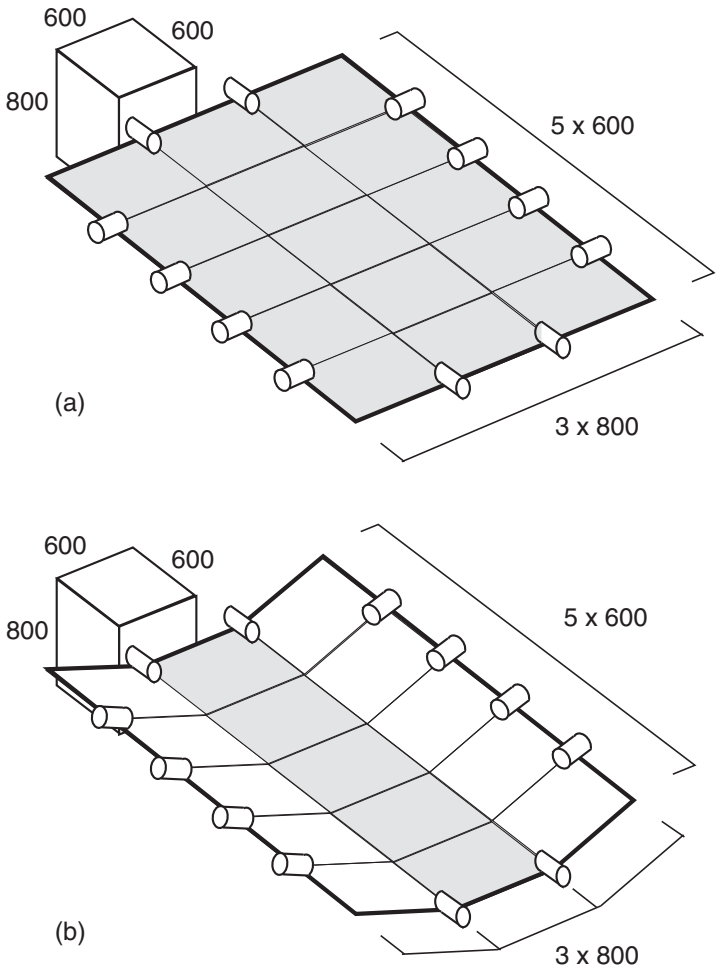

Figure 3.1: Schematic configuration of solar-array structures.

hinge lines by rotating the edge panels through 180°. Thus, the structure folds transversally with the side panels being folded above and below the central panels. Then, the transverse hinges are activated to Z-fold the structural longitudinally. The whole sequence can be visualised by following *in reverse* the sequence in Figure 3.2.

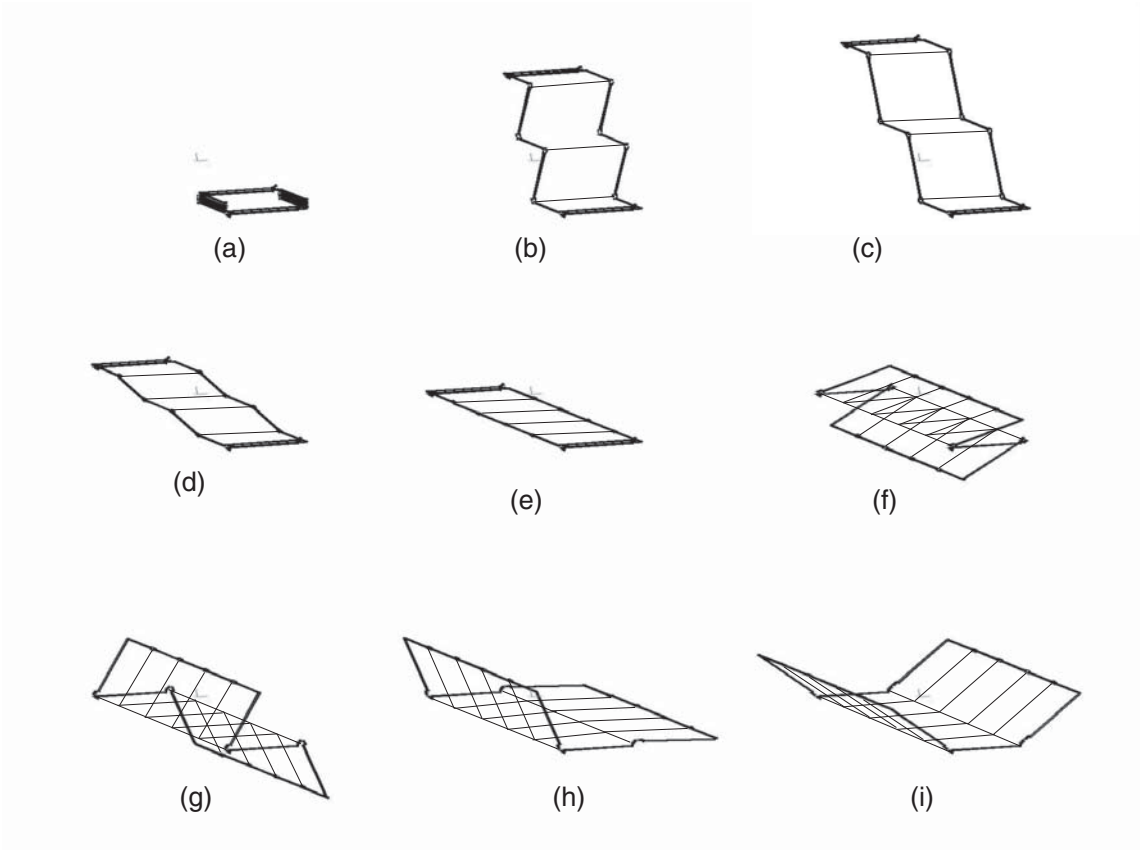

Figure 3.2: Deployment simulation of concentrator array; (a–e) longitudinal deployment, (f–i) deployment of side panels.

Because of the small thickness of the panels, it is not difficult to arrange the hinges between the panels to permit this bi-axial folding. However, designing an edge frame that folds in a manner compatible with the panels is more challenging and, to verify that it is possible, a simple physical model was designed and constructed.

This model, shown in Figure 3.3, consists of a 0.98 (0.85 on the shorter side)$\times$0.7 m^2 timber frame, made from 25×32 mm^2 rectangular section members connected by brass hinges, to which a thin foil has been attached with double-sided adhesive tape.

Note that, whereas the hinges that allow Z-folding of the longitudinal members are *surface-mounted*, the hinges in the transverse members are mounted half-way through the thickness

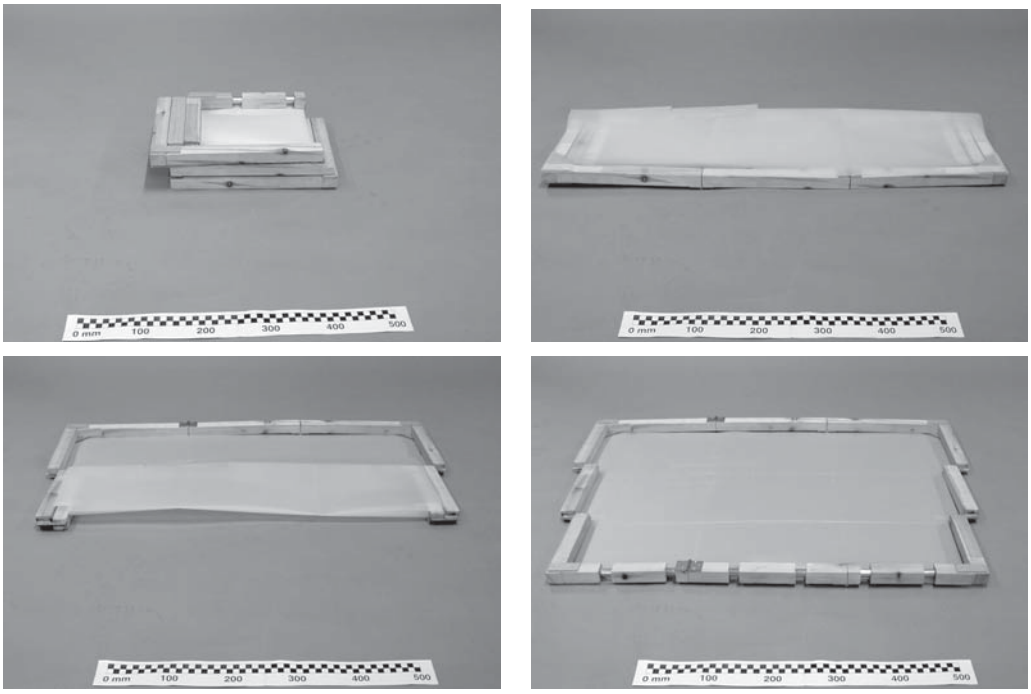

Figure 3.3: Deployment of model structure.

of these members. This is required to avoid that thickness of the frame trebling after it has been folded transversally; if this happened the hinges that allow Z-folding would no longer be co-planar and so the folding would not work.

This kinematic model demonstrates the viability of the proposed concept although, of course, further work will be needed to transform it into a proper structure.

By changing the configuration of the TSR hinges in the transverse members, the same model can be used to produce the trough configuration already seen in Figure 3.1(b). This is shown in Figure 3.4.

3.2 Analysis of Flat Array

In order to obtain preliminary estimates for the sizes of the members of the deployable frames, and thus estimate their mass, both configurations of the solar array were analysed using Pro/Mechanica (2000). This section presents the results obtained for the flat array.

It was assumed that all members are hollow tubes made of CFRP (E=100 GN/m^2, ρ=1500 kg/m^3). The mass of the panels, 2.1 kg/m^2 giving an overall mass of 15.12 kg, was modelled as four equal masses at the corners of the frame. The 12 self-locking hinges between the members of the frame were assumed to be TSR hinges of the same type as those described in Section 3.2.1.

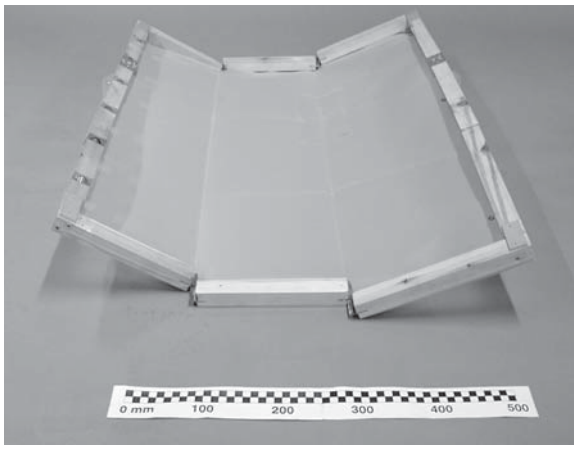

Figure 3.4: Model structure in concentrator configuration.

As the overall design of a deployable structure is based primarily on a stiffness requirement, the lowest natural frequencies of several possible designs of the deployable frame were compared. In all cases it was assumed that the central element of one of the transverse members is rigidly connected to the spacecraft bus.

A first analysis was carried out for members with outer diameter (o.d.) of 25 mm and 1 mm wall thickness ($I = 5438$ mm^4). The mode shapes for the structure with TSR hinges are shown in Figure 3.5. Note that the first two modes, at 0.44 and 0.60 Hz, involve out-of-plane bending and in-plane shearing of the frame. The third mode is a twisting mode.

It is interesting to compare the first four natural frequencies of the frame with TSR hinges to the corresponding frequencies of a rigidly-jointed frame, see Table 3.1. It can be seen that the lowest natural frequency of the frame increases only by 10%.

Mode	TSR Hinges	Stiff Hinges
1	0.44	0.49
2	0.60	0.83
3	1.04	1.14
4	2.76	4.88

Table 3.1: Natural frequencies (Hz) of flat solar array with 25 mm o.d. and 1 mm thick CFRP tubes.

If a higher fundamental natural frequency is required, stiffer tubes are needed. As the bending stiffness of circular tubes increases approximately with the cube of the radius and only linearly with the thickness, an increase in stiffness is best gained by increasing the radius.

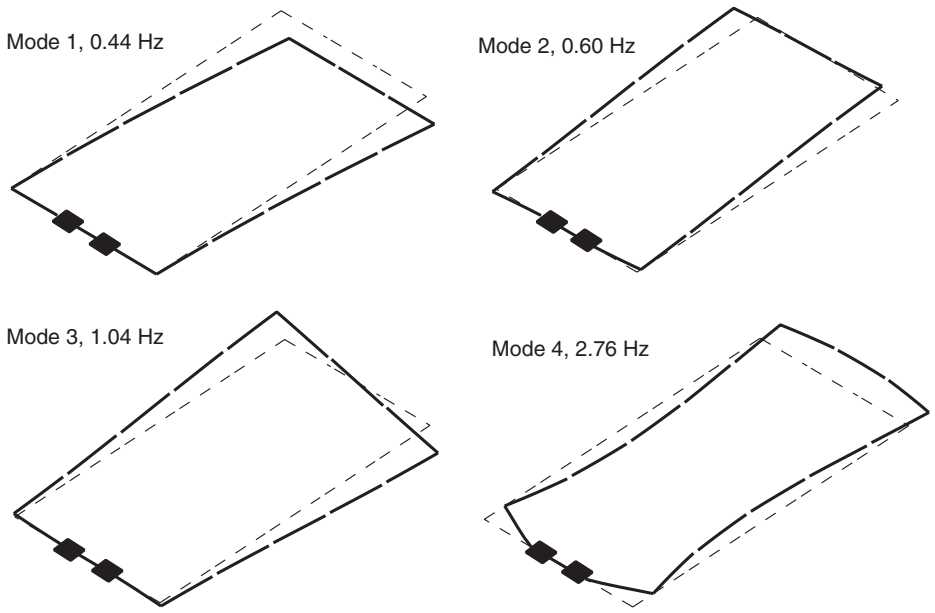

Figure 3.5: Natural modes of flat solar array structure with 25 mm o.d., 1 mm thick tubes connected by TSR hinges.

Therefore, an alternative design with 50 mm o.d. tubes with 1 mm wall thickness was considered. The corresponding mode shapes, for the frame with TSR hinges, can be seen in Figure 3.6. Table 3.2 compares the first four natural frequencies of frames with TSR hinges to frames with full connections.

Mode	TSR Hinges	Stiff Hinges
1	0.79	1.84
2	0.82	3.08
3	2.09	4.32
4	3.21	17.6

Table 3.2: Natural frequencies (Hz) of flat solar array with 50 mm o.d. and 1 mm thick CFRP tubes.

In this analysis the fundamental natural frequency of the TSR hinge frame is approaching 1 Hz, however the stiff hinge model shows a fundamental natural frequency significantly over 1 Hz indicating that the flexibility of the frame arises primarily from the flexibility of the hinges. This suggests that a more efficient frame could have tubes of smaller radius and stiffer TSR hinges.

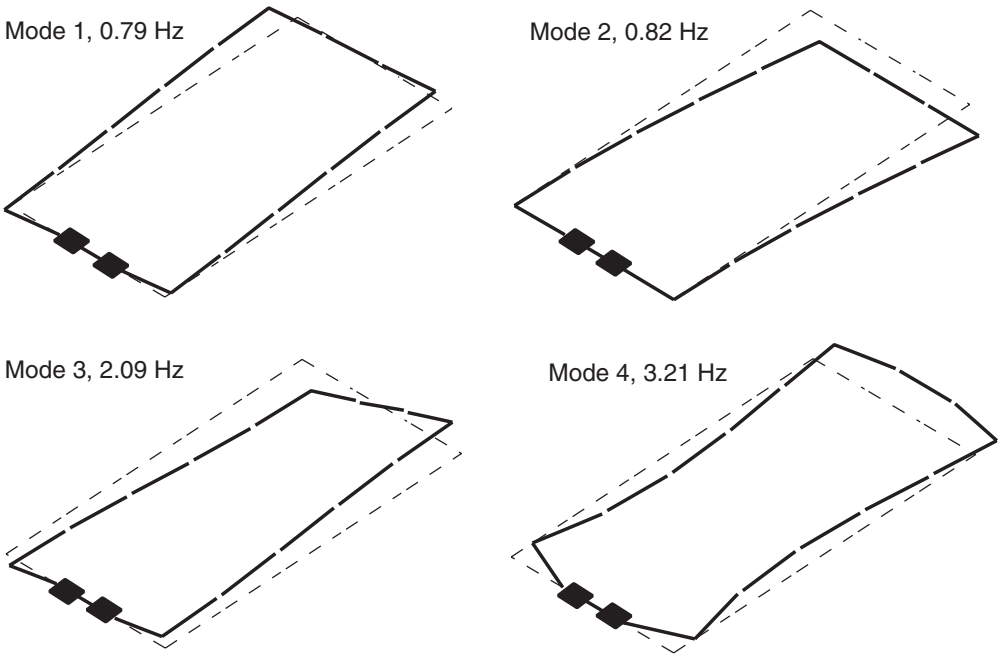

Figure 3.6: Natural modes of solar array frame with 50 mm o.d. and 1 mm thick members, connected by TSR hinges.

3.2.1 TSR Hinges

Tape Spring Rolamite (TSR) hinges consist of short lengths of Sears steel tape measure, and rolling elements—made from Delrin, a space qualified acetal resin—connected by steel cables, Figure 3.7. Hinges made on this concept have already been made and their mass is typically ≈ 100 g each.

Because the stiffness properties of a TSR hinge can be modified to meet different requirements, two different hinge models were used in the analysis. The first model assumes that the

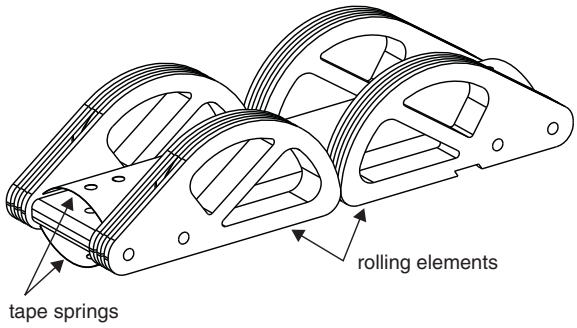

Figure 3.7: Tape-Spring Rolamite hinge.

hinge is practically infinitely stiff, and thus provides an upper bound on the fundamental natural frequency that can be achieved for a given mass of the membrane without increasing the stiffness of the members. The second model uses the stiffness values that were estimated by Watt (2000) for a particular design of the TSR hinge. The stiffness values used in the two models are given in Table 3.3. Each hinge, complete with end fittings, is assumed to be 100 mm long and to have a mass of 150 g.

Direction	Stiff Hinges	TSR Hinges	Units
Axial	1×10^9	9.6	kN/mm
Shear in plane of tape springs	1×10^9	3.24	kN/mm
Shear perpendicular to tape springs	1×10^9	10.4	kN/mm
Twisting	1×10^{10}	10	MNmm/rad
Bending about axis of hinge	1×10^{10}	1.68	MNmm/rad
Bending perpendicular to axis of hinge	1×10^{10}	1	MNmm/rad

Table 3.3: Hinge stiffnesses used in Pro/Mechanica model.

In Pro/Mechanica a TSR hinge is modelled as a spring element between the end nodes of the two beam elements to be connected, which are located 100 mm apart. Two point masses at the end of each spring model the mass of the hinge.

3.3 Analysis of Array with Concentrator

Several designs of the array with concentrator elements were similarly analysed with Pro/Mechanica. The use of concentrators lowers the mass of the solar array to an average of 0.873 kg/m^2 (giving a total mass of 6.3 kg), excluding the frame. The mass of the tubes and hinges remains unchanged.

An analysis was made of a trough shaped frame structure where the mass of the panels covered with photovoltaic cells is concentrated at the corners of the central part of the trough. Round CFRP tubes with 25 mm o.d. and wall thickness of 1 mm, as before, were used all around and the frame was analysed assuming either TSR hinges or built-in connections between the members. The first four mode shapes of the frame with TSR hinges can be seen in Figure 3.8 and the natural frequencies are compared in Table 3.4 to the corresponding frequencies of the rigidly-jointed frame.

The fundamental natural frequency is 40% higher than for the flat frame with TSR hinges, due to the lower mass of the panels. Comparing the natural frequencies of the frame with TSR

hinges to those of a frame with rigidly-jointed connections, it is found that—as for the flat array—the two sets of frequencies are quite close, which suggests that the frame flexure arises from a lack of stiffness in the beam members. For this reason a second analysis using 50 mm o.d. 1 mm thick round CFRP tubes was made with both stiff hinges and TSR hinges as before. The first four natural frequencies are listed in Table 3.5.

Mode	TSR Hinges	Stiff Hinges
1	0.62	0.72
2	0.84	1.10
3	2.56	2.84
4	3.19	4.24

Table 3.4: Natural frequencies (Hz) of concentrator solar array frame with 25 mm o.d. and 1 mm thick CFRP tubes.

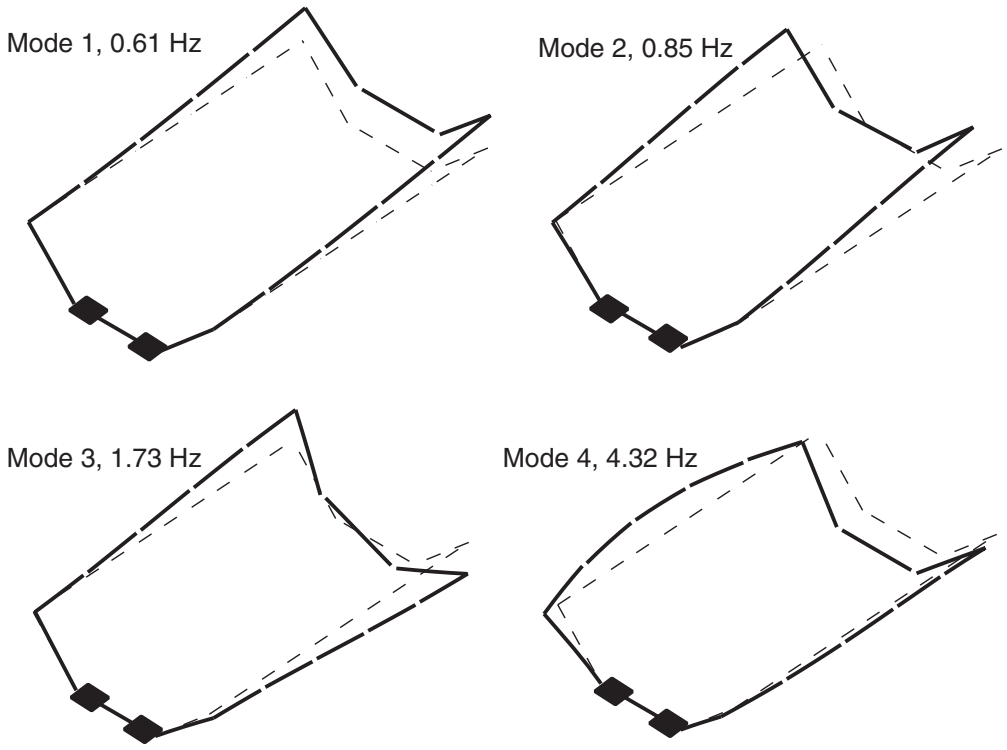

Figure 3.8: Natural modes of solar array concentrator frame with 25 mm o.d. and 1 mm thick tubes, connected by TSR hinges.

Mode	TSR Hinges	Stiff Hinges
1	1.02	2.00
2	1.17	3.03
3	4.36	7.51
4	4.47	11.81

Table 3.5: Natural frequencies (Hz) of concentrator solar array frame with 50 mm o.d. and 1 mm thick CFRP tubes.

3.4 Mass Estimates

Mass estimates for the two types of solar array structures are presented in Tables 3.6 and 3.7. In both cases it has been assumed that the smaller diameter tubes (25 mm o.d.) are adequate.

Element	Quantity	Unit Mass	Mass (kg)
Membrane	7.2 m^2	2.1 kg/m^2	15.12
Hinges	12	0.15 kg	1.8
Round tube beams (25 mm o.d.)	10.8 m	0.058 kg/m	0.63
Total			17.55

Table 3.6: Mass breakdown for membrane solar array (kg).

Element	Quantity	Unit Mass	Mass (kg)
Membrane	2.4 m^2	2.1 kg/m^2	5.04
Concentrator	4.8 m^2	0.26 kg/m^2	1.25
Hinges	12	0.15 kg	1.8
Round tube beams (25 mm o.d.)	10.8 m	0.058 kg/m	0.63
Total			8.72

Table 3.7: Mass breakdown for concentrator membrane solar array (kg).

3.5 Discussion

A packaging scheme for a 1.5 kW solar array that can be folded alongside a $0.6 \times 0.6 \times 0.8 m^3$ STRV-type spacecraft has been presented. The packaged volume of the structure is approximately $0.6 \times 0.8 \times (0.025 \times 5)$ m^3 and its mass either 17.5 kg, if a flat array configuration is selected, or 9 kg for a concentrator array.

After completing this study it was noticed that a more efficient design for the concentrator array may be that shown in Figure 3.9. Here the edge frame has been replaced with a narrower deployable frame that supports the heavier panels, i.e. those with photovoltaic cells. These panels would be attached directly to the frame and would no longer need to be fastened to prestressed wires.

The lighter concentrator panels would be supported by tension wires attached to foldable arms that are connected by the TSR hinges to the corners of the deployable frame. Because the concentrator panels are much lighter, only a small amount of prestress—around 20 N—would be required to prevent a set of five concentrators strung together from vibrating at a frequency lower than 1 Hz.

It is recommended that this alternative scheme be further investigated.

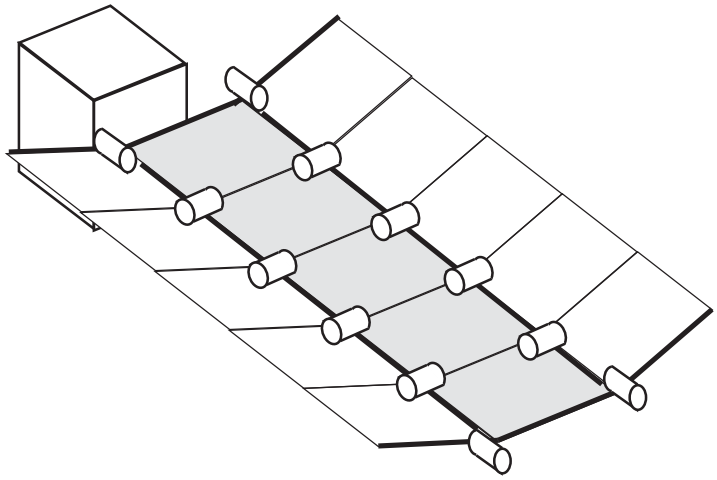

Figure 3.9: Alternative design of concentrator array.

Chapter 4

Deployable Reflector

A potential application has been identified for a 3 m diameter parabolic reflector with a focal length to diameter ratio $F/D = 0.4$, to operate at a frequency of 9.65 GHz (a value of 10 Ghz will be used).

4.1 Background

The authors are not aware of any existing deployable reflector system that would be suitable for the present application. This is excluding inflatable reflectors, on which much work is currently being done in the USA, but still cannot be regarded as a mature technology. Of the existing technologies, it is considered that an adaptation of a concept first proposed by Miura (1986) for the 8 m diameter Muses-B spacecraft and then most elegantly implemented by the Astro Aerospace Corporation (Thomson 1997), now TRW Astro, offers the greatest potential for meeting the requirements with a low-cost system.

Realising a doubly-curved furlable mesh surface is expensive and technically challenging. Only companies that have built up a considerable know how in this field, such as the Harris Corporation, are capable of delivering trouble-free reflector structures based on this approach, albeit at a high cost. Also, the implementation of an umbrella-type concept for an application with the severe packaging requirements of the present application would be very complex.

An alternative is to aim for a triangulated surface that approximates to the required paraboloidal surface, supported by a network of thin cables, or tapes with high axial stiffness. The cables are prestressed to form a stiff and accurate structure, which Miura (1986) called a *tension truss*. The size of the triangles forming the cable network is chosen sufficiently small to achieve the required accuracy. The first implementation of this concept was the Tension Truss Antenna

(Miura and Miyazaki 1990), in which the triangulated net was supported by six telescopic masts.

A recent implementation of this approach is the AstroMesh Reflector, Thomson (1997), see Figure 4.1. Here the forces that are required to prestress the cable network are provided by a series of springs, called tension ties, connecting the network to an identical rear net. Both networks are connected around the edge to a deployable ring truss with telescopic diagonals.

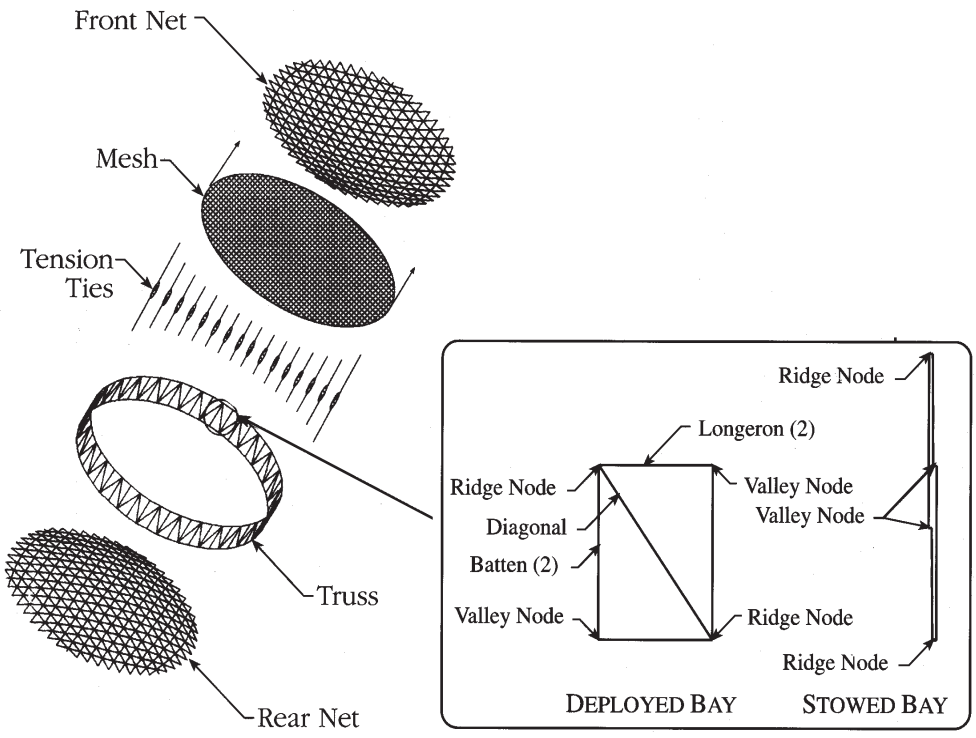

Figure 4.1: AstroMesh concept.

Note that the height of the ring truss is given by the depth of the two nets plus their separation. Although the rear net can be made less deep, say half the depth of the front net, by accepting larger forces on the ring, a reflector with small F/D requires a high ring. For example, for a reflector depth $H = 0.46$ m and $D = 3$ m an AstroMesh-type truss divided into 18 segments would have a packaged height of more than 1.2 m. An alternative ring configuration, based on a pantograph with, again, 18 bays would have a height of 0.9 m. However, this requires a large number of joints.

For the reasons stated above it was concluded that a new concept was needed in order to meet the present requirements. Hence, Section 4.2 of this report presents the concept that has

been developed. Simple demonstrator hardware has been made to illustrate the concept and demonstrate its viability. Section 4.5 briefly describes a 3 m reflector that would meet all the DERA requirements and goes on to obtain initial mass estimates.

4.2 A New Concept

The proposed reflector structure is based on the tension truss concept. Like the AstroMesh, it is composed of three main parts:

- a deployable ring structure;
- two identical cable nets (front and rear nets) connected by tension ties;
- the reflecting mesh, attached to the front net.

Although the concept is a general one, for clarity it will be explained with reference to the particular example shown in Figure 4.2. Basically, we are dealing with a structure consisting of a large number of cable elements and constant-tension springs with only six struts (compression elements).

Figure 4.2(a) highlights the 18 cable elements and 6 struts that form the *deployable ring structure*. This is a well-known "tensegrity structure" belonging to a family invented in 1948 by the sculptor Kenneth Snelson and by R. Buckminster Fuller. Two important features of tensegrity structures are that:

- There is no connection between compression elements;
- The connections between compression and tension members are simple.

These features make them particularly attractive in applications requiring low-weight, low-cost deployables that can be packaged very compactly. A disadvantage of standard tensegrity structures is that they are very flexible, due to the existence of internal mechanisms of inextensional deformation, as will be shown next. However, we have obtained a new solution that avoids this problem.

Consider the pin-jointed structure shown in Figure 4.3, whose layout is identical to the ring structure in Figure 4.2. The top six joints lie at the corners of a regular hexagon and the bottom six joints lie at the corners of an identical hexagon. Each joint is connected by bars to the two neighbouring joints in the same hexagon, and also to two joints of the top hexagon. Note that it is not connected to the joint directly above, but to the next and the second next joints, in an anti-clockwise sense.

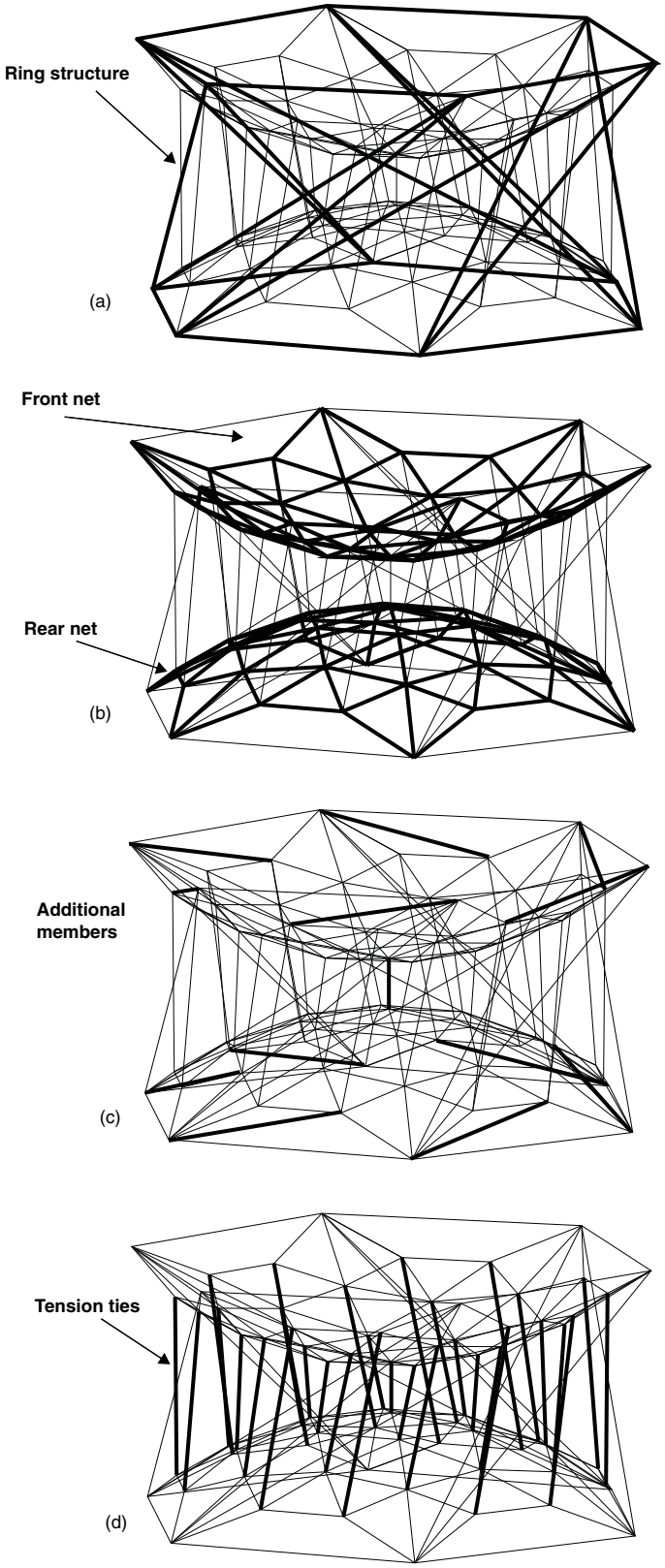

Figure 4.2: New concept.

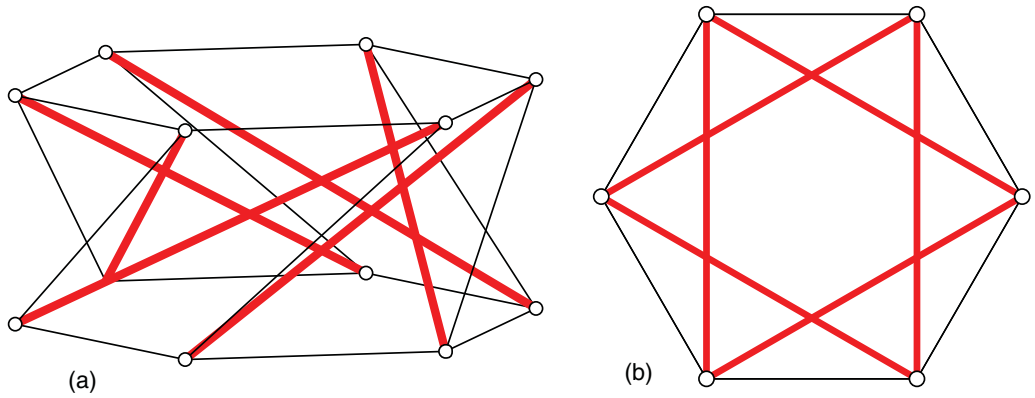

Figure 4.3: Hexagonal tensegrity module; (a) three-dimensional view; (b) top view.

This structure has $j = 12$ joints and $b = 24$ bars. To investigate its static and kinematic properties we use the extended Maxwell's rule (Calladine 1978)

$$3j - b = m - s \tag{4.1}$$

where

- $m =$ number of independent inextensional mechanisms, and
- $s =$ number of independent states of self-stress

Substituting the values of j and b into Equation 4.1 we obtain

$$m - s = 12 \tag{4.2}$$

It can be shown that this structure has one state of self-stress, $s = 1$, where the six longer bars connecting the two hexagons are in compression and all other members are in tension. Therefore, from Equation 4.2 we conclude that $m = 13$ and, since six mechanisms will be rigid-body motions of the whole structure, this leaves seven internal mechanisms. These mechanisms can be stiffened by prestressing the structure, but this will only provide a relatively small amount of stiffness.

Because this structure can be prestressed, as described, a deployable version can be made quite easily. The state of prestress will require only six members to carry compressive forces, all other members are in tension and therefore—instead of using bars—they can be replaced with cables. Then, if the struts are collapsible, e.g. either telescopic or foldable at a series of hinge points, the whole structure can be folded.

This structure, however, has seven internal mechanisms, which is clearly undesirable. Therefore, we have modified it by connecting two identical triangulated structures to the hexagons, as shown in Figure 4.2(b); the layout of these nets is more clearly shown in Figure 4.4.

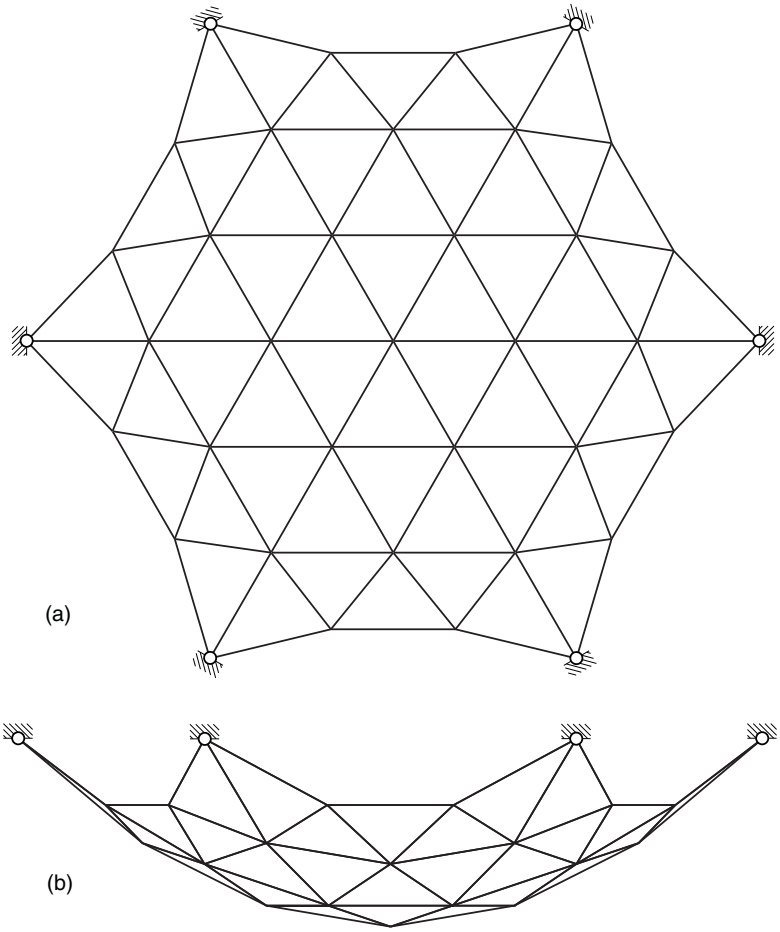

Figure 4.4: (a) Top and (b) side views of front and rear nets.

The layout of these nets can be defined in many different ways, for example it could be optimised such that all triangles have equal area and are as close as possible to equilateral. The particular layout that was chosen is based on a simple two-dimensional, regular tessellation of equilateral triangles that is obtained by dividing each side of a hexagon into three. Then, the outermost triangles were distorted to form a catenary-like edge for the net to improve the force distribution in it. Finally, all nodes were projected onto a paraboloid. See Section 4.3 and the Appendix for more details.

Consider the structure consisting of the original ring structure plus the two triangulated nets; its static and kinematic properties are investigated as follows.

- Number of joints: there are 6 joints in the symmetry unit of each net, hence

$$j = 2 \times (1 + 6 \times 6) = 74 \tag{4.3}$$

- Number of bars: there are 15 bars in the symmetry unit of each net, plus the 24 bars of the ring structure, hence

$$b = 2 \times (15 \times 6) + 24 = 204 \tag{4.4}$$

Substituting Equations 4.3 and 4.4 into Equation 4.1 we obtain

$$m - s = 18 \tag{4.5}$$

Since the state of self-stress is still statically possible, but no additional states of self-stress have been created, we have $s = 1$. Hence, $m = 19$ and, of these mechanisms, 6 are rigid-body motion and 13 internal. The 13 internal mechanisms can be removed by adding 13 bars to the structure, as shown in Figure 4.2(c). The resulting structure has $m = 6$, and hence only rigid-body mechanisms, and $s = 1$.

To realise this structure in practice we need to find a way of prestressing the two nets. The obvious way of doing it is to connect corresponding nodes of the two nets with a series of tension ties that apply equal forces. It turns out that this is not an ideal solution because

1. large compressive forces are induced in the cables of the ring structure, which need to be counteracted by increasing the level of prestress of the ring; this would further increase the compression in the struts;[1]

2. 12 of the 13 additional members shown in Figure 4.2(c) are not pre-tensioned;

It was found that all of these issues can be resolved by modifying the configuration of the ring structure. Instead of using the original configuration, where the two hexagons are directly one above the other as shown in Figure 4.3(b), one hexagon is rotated through a small angle, Figure 4.5.

By itself, the resulting ring structure can no longer be prestressed, as $s = 0$ and hence, from Equation 4.2, $m = 12$. However, when the structure is considered in its entirety, including the prestressing forces applied by the tension ties, the following is found.

- To obtain a structure free of internal mechanisms only 12 additional members are required, not 13, hence the member connecting the centres of the two nets can be replaced with a tension tie.

[1] It will be seen in Section 4.3 that the forces predicted by a linear analysis of the ring structure become infinite.

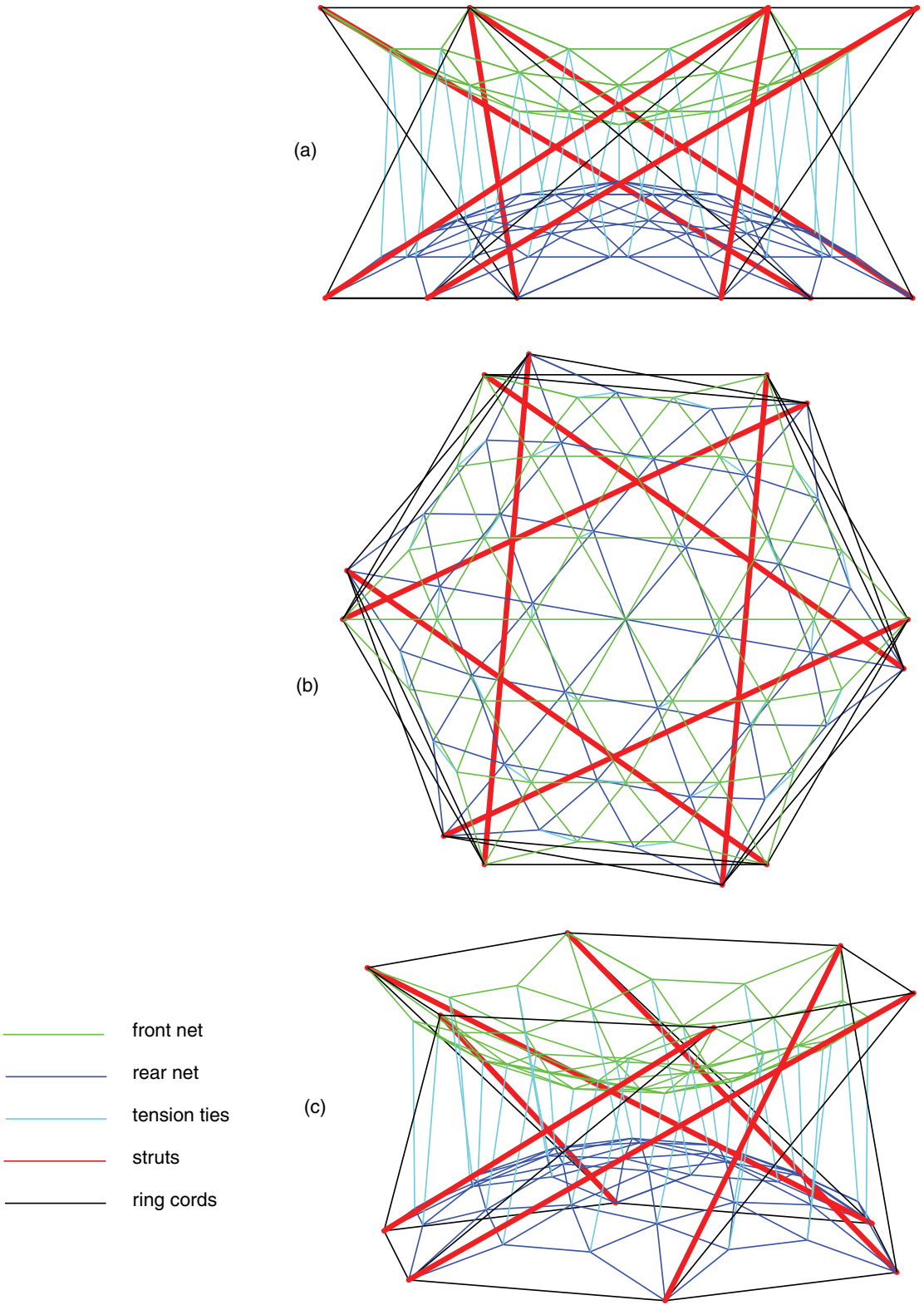

Figure 4.5: Complete structure, additional 12 members not shown.

- For a 10° anti-clockwise rotation of the upper hexagon with respect to the bottom hexagon—as shown in Figure 4.5—all of the cables are in a state of tension.[2]

Figure 4.6 shows the force distribution in the two nets; the corresponding forces in the ring structure are −68.8 N in the struts, +25.9 N in the cables forming the hexagons, and +39.5 N in the six cables linking the hexagons.

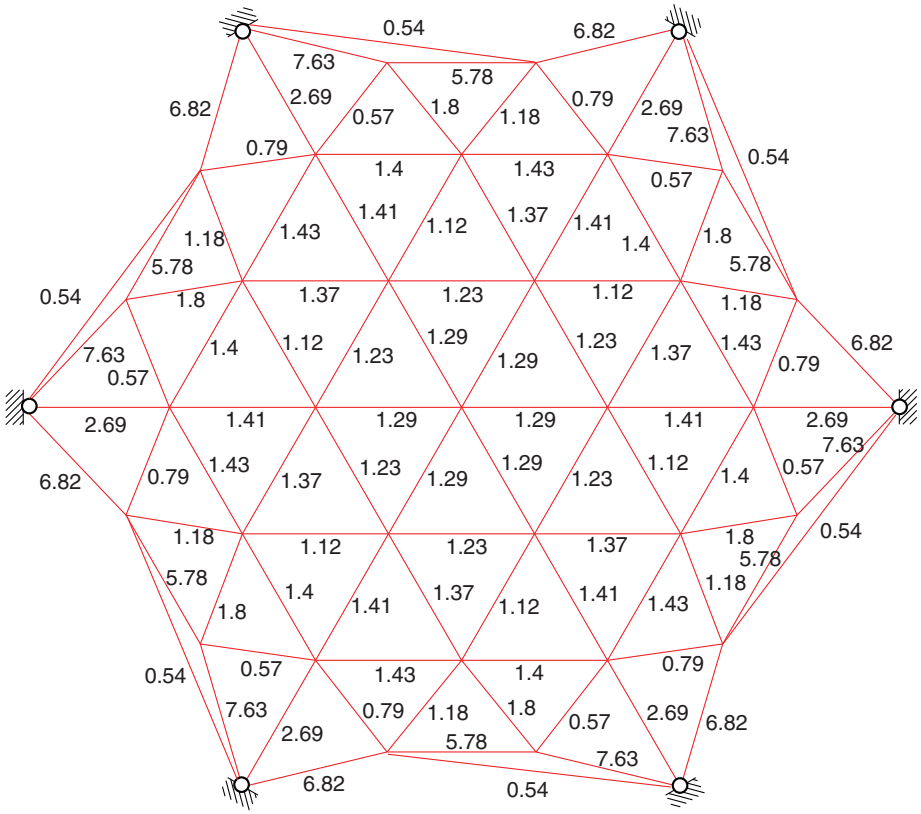

Figure 4.6: Force distribution in the two nets due to tension tie loads of 1 N on the inner nodes and 2 N on the edge nodes.

4.3 Configuration of Tensegrity Reflector

In addition to studying the statical and kinematical properties of the reflector structure, it is necessary to analyse the effect of different design parameters on the magnitude and distribution of the forces within the structure. Our aim is to obtain a fairly uniform distribution of forces

[2]Note that the forces in the outer ties have been set to twice the value of the internal ties.

in the net and to avoid large forces in the supporting structure, particularly the struts. The configuration study is divided into two parts. First, the influence of the sag-to-span ratio of the net edges and the tension ties forces on the forces in the net is investigated. Then, for some particular values of the forces in the tension ties and a particular sag-to-span ratio, the effect of the relative rotation of the hexagons on the forces in the nets and the ring structure is considered.

A detailed description of the procedure used for generating the triangular net mesh and how the sag-to-span ratio is defined are given in the appendix at the end of this chapter.

4.3.1 Effects of Sag-to-Span Ratio and Tension Tie Forces on Net Forces

Throughout this first study the tension ties are represented by vertical loads on the joints of the net, see Figure 4.7. We begin by checking the statical and kinematical properties of the three-ring cable net in Figure 4.7. From the Appendix, the number of joints is

$$b = 6\frac{3(1+3\cdot 3)}{2} = 90 \tag{4.6}$$

and the number of bars is

$$j = 1 + 6\frac{3(1+3)}{2} = 37 \tag{4.7}$$

The extended Maxwell's rule, Equation 4.1, yields

$$m - s = 21 \tag{4.8}$$

From the synclastic shape of the net, it is obvious that no state of self stress can be sustained giving $s = 0$. By fixing 6 joints in space we get $m = 3$. Hence, we need to fix another three degrees of freedom to eliminate the internal mechanisms. Following Pellegrino (1993) we have analysed the equilibrium matrix of the structure and thus computed three independent mechanisms. By looking at plots of these mechanisms we decided to fix one edge joint radially and tangentially, i.e. two perpendicular in-plane directions, and its neighbouring edge joint radially. This gives a statically and kinematically determinate structure.

The cable net in Figure 4.7 was analysed for three sag-to-span ratios: 5, 10 and 15%. For each ratio the initial setting of the tension tie forces was 1 N everywhere, which is most practical as identical constant-tension springs would be used in all of the tension ties. However, if the force pattern in the net is irregular or, worse, some elements are in compression, the tension tie forces have to be adjusted.

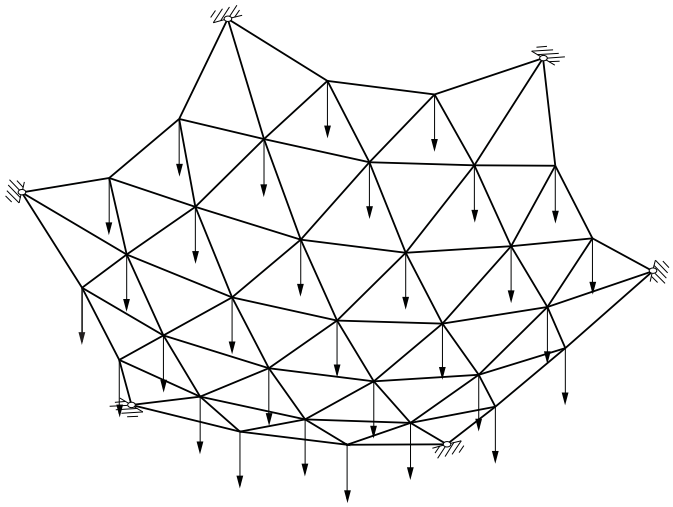

Figure 4.7: Loads applied to cable net to study the influence of sag-to-span ratios on the force pattern.

The results for a 5% sag-to-span ratio are shown in Figure 4.8. For the case where the tension tie forces are all equal to 1 N, Figure 4.8(a), some members are in compression. By increasing the edge forces the compressive forces gradually become smaller and then tensile, Figure 4.8(b)–(d), as the edge forces are increased. An almost uniform force distribution is obtained for edge forces of 4 N, however the largest force in the edge cable is now over 15 N.

When the sag-to-span ratio is increased to 10% there is still compression for tension tie forces of 1 N, Figure 4.9(a). However, as the force in the edge ties is increased to 2 N an acceptable distribution of net forces is obtained and the edge forces are smaller than for the 5% sag-to-span ratio, Figure 4.9(b). The range of the inner net forces is 0.75–2.69 N.

Increasing the sag-to-span ratio further to 15% yields no compressed elements even for the case of uniform 1 N tension tie loads, Figure 4.10(a). By increasing to 2 N the forces in the edge ties gives a very uniform force pattern, in the range 1.27–2.08 N, and the edge cable forces are slightly smaller than in the previous case.

Although a sag-to-span ratio of 15% gives a better force pattern than the 10% ratio, the further loss of reflecting area is not justified, hence 10% is the value that is selected.

4.3.2 Rotation of hexagons

Next, the effect on the prestress distribution of a relative rotation θ between the hexagons of the ring structure is analysed, assuming that the cable nets have a fixed sag-to-span ratio of 10%. The tension tie force is 1 N on the inner joints and 2 N on the edge joints, giving the

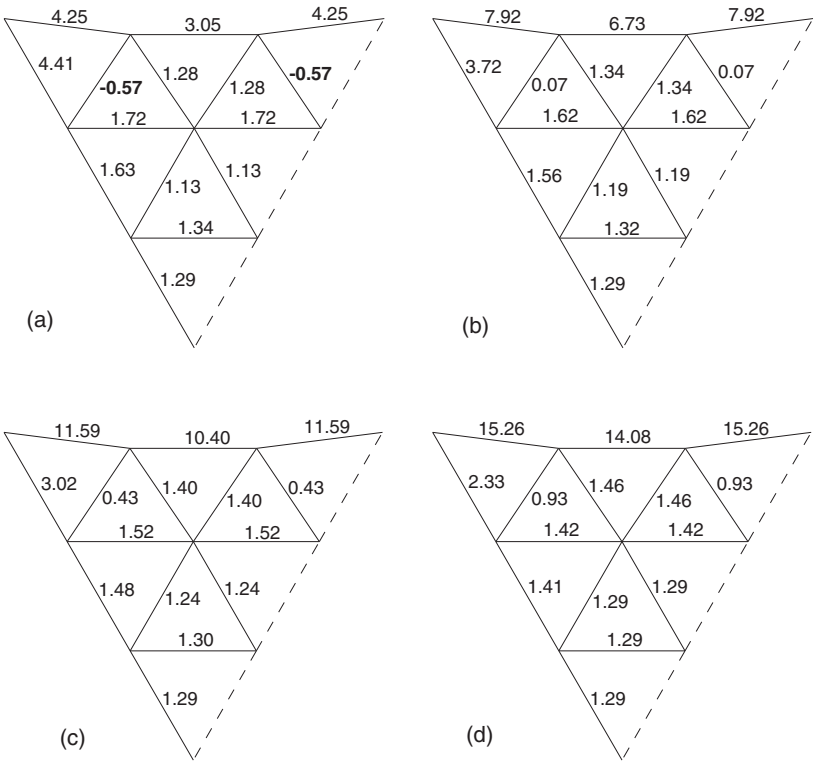

Figure 4.8: Forces in a net with 5% sag-to-span ratio. Loads on inner nodes: 1 N; loads on edge nodes (a) 1 N, (b) 2 N, (c) 3 N, (d) 4 N.

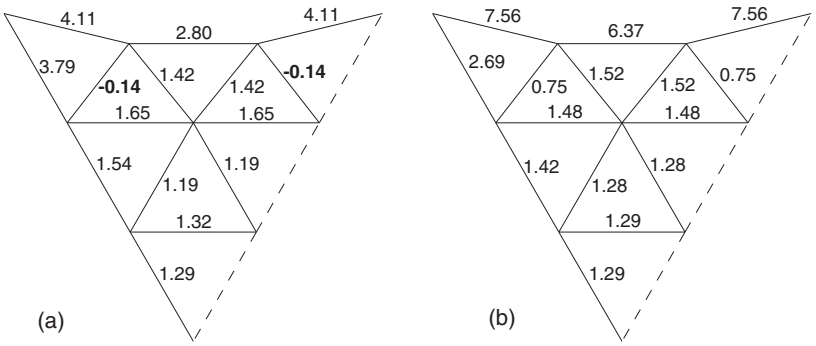

Figure 4.9: Forces in a net with 10% sag-to-span ratio. Loads on inner nodes: 1 N; loads on edge nodes (a) 1 N, (b) 2 N.

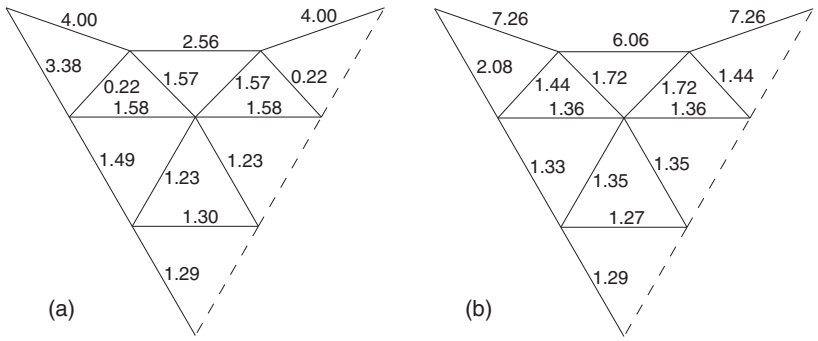

Figure 4.10: Forces in a net with 15% sag-to-span ratio. Loads on inner nodes: 1 N; loads on edge nodes (a) 1 N, (b) 2 N.

force distribution shown in Figure 4.9(b) for $\theta = 0$. However, when the hexagons are rotated, the force distribution in a bay of the net is no longer symmetric, Figures 4.11 and 4.12.

Net forces

Figure 4.11 plots the variation in the forces of the inner net elements with the rotation of the hexagons. The forces in the radial cables 1, 3 and 8 are approximately constant, for the range of θ displayed. The other cable forces—except for cables 9 and 10—are within 0.5–1.5 N. Most importantly, cable 9 becomes compressed at $\theta \approx 28^\circ$ giving an upper limit on θ for the particular reflector configuration studied here.

Figure 4.12 plots the variation in the forces of the edge elements. The force in edge cable 13 initially increases and then decreases. Edge forces 14 and 15 decrease when θ is increased. This is due to the change in the direction of the tension tie forces.

Ring forces

The element forces in the ring structure vary exponentially with θ, Figure 4.13. For small angles, the forces are far too large, especially in the struts. It is not until we reach $\theta = 10^\circ$ that the forces have decreased to an acceptable level. Further rotation decreases the force, although much more slowly, and for the practical limit of 28°, discussed above, the force in the lateral cables is 3.9 N. Note that the structure is statically and kinematically determinate and, therefore, is not dependent on the prestress level for stiffness. However, the cables must be tensioned to a sufficient level that they are able to take compressive loads without going slack.

Also shown in Figure 4.13 is the variation of the strut length, which is not as dramatic as the strut forces, although shorter struts are preferable.

Additional members

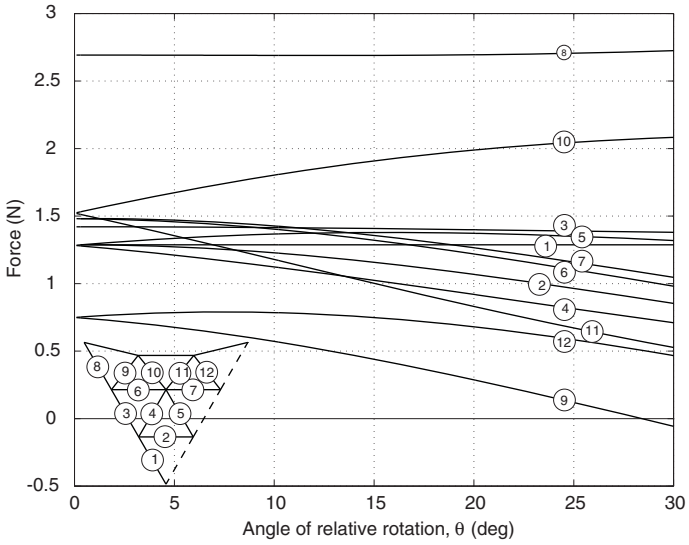

Figure 4.11: Variation of forces in net cables.

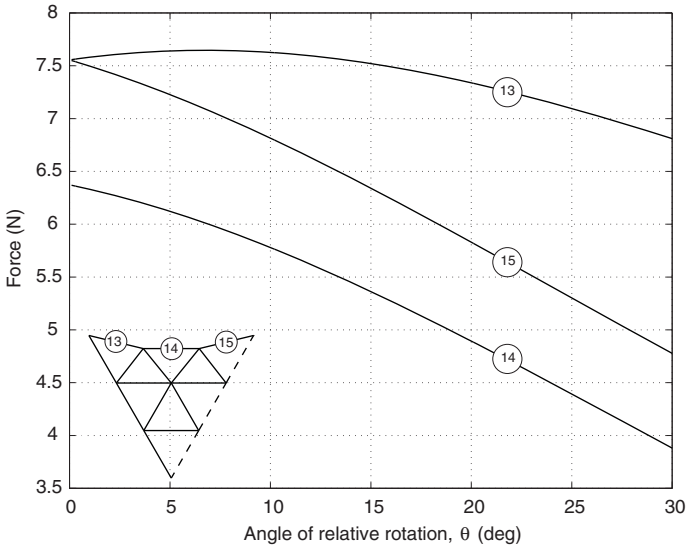

Figure 4.12: Variation of forces in edge cables.

The additional elements, shown in Figure 4.2(c), were added to make the structure statically and kinematically determinate but, of course, they need to be pre-tensioned if cables are to be used. In the current configuration of these elements, it turns out that they are always in tension when the hexagons are rotated, Figure 4.14, and the magnitude of the tension increases almost linearly up to about 10°. However, if the additional members were re-arranged from an anti-clockwise direction (defined from edge joints to ring joints) to clockwise they would be in compression, instead.

Other issues

Another important issue, not concerned with the force distribution within the structure, is that the struts move closer to the centre of the reflector when θ is increased. Hence, the struts are more likely to interfere with the tension ties. This might complicate the deployment procedure; therefore, it is important to keep θ small.

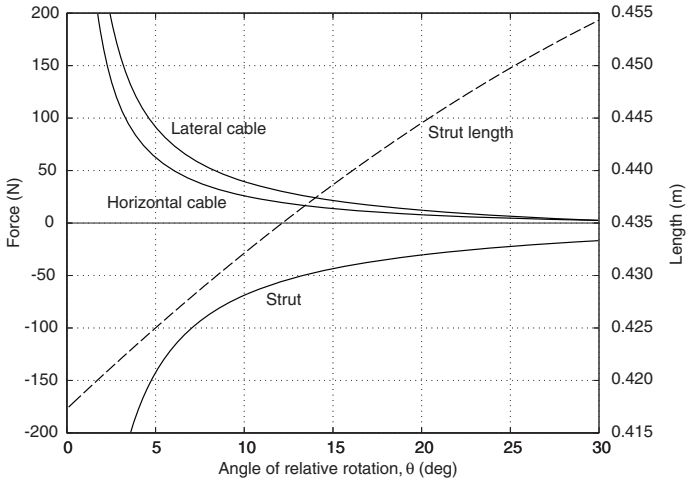

Figure 4.13: Variation of forces in ring structure.

4.4 Demonstration model

To verify the feasibility of the proposed concept, a small-scale physical model was constructed, with a diameter of 0.47 m.

The nets for the model were constructed on paraboloidal molds of PETG (a thermo-plastic material with the trade name of Vivak) with diameter $D = 0.45$ m and focal length $F = 0.134$ m, on which the position of the nodes of the net had been marked with a 3-axis CNC machine. The members of the net were 0.8 mm diameter Kevlar cords which were pretensioned before being taped to the mold; then, the cords were joined at all cross-over points by Nylon loops

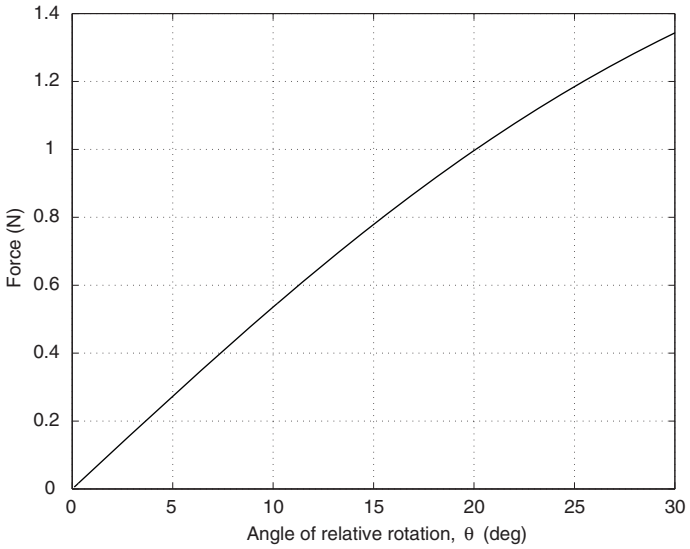

Figure 4.14: Variation of forces in additional members.

and bonded with epoxy resin. Corresponding nodes of the two nets were connected with rubber bands, later replaced with steel springs.

Identical Al-alloy, 30 mm long joint fittings of cylindrical shape with a diameter of 15 mm, were attached to the six corners of each net. These fittings had been precision drilled with 2.0 mm diameter holes in the directions of all the cords that need to be connected to a node, and all connections were made with epoxy resin. The cords of the ring structure, also attached to the same joint fittings, were made from 1.0 mm Kevlar cord.

To "deploy" the model, 0.46 m long Al-alloy struts are inserted into 20 mm long, 6.4 mm diameter holes that are co-axial with each fitting and are fastened with a grub screw. Photographs of the deployed structure are shown in Figure 4.15.

The model works quite well, considering that it was the first attempt at putting together a structure of this kind. However, some of the net cables are slack and there is some interference between the nets and the struts, because the diameter of the net—as manufactured—turned out to be bigger than expected. Correcting these problems should not be difficult when a new model is made.

It is envisaged that the struts will be made collapsible by inserting a series of self-deploying, self-locking hinges but, for the time being, the folding process has been simulated by replacing the struts with 0.12 m long wood dowel. Figure 4.16 shows the very compact packaged configuration; note the elongated shape of the package, compatible with the DERA requirements.

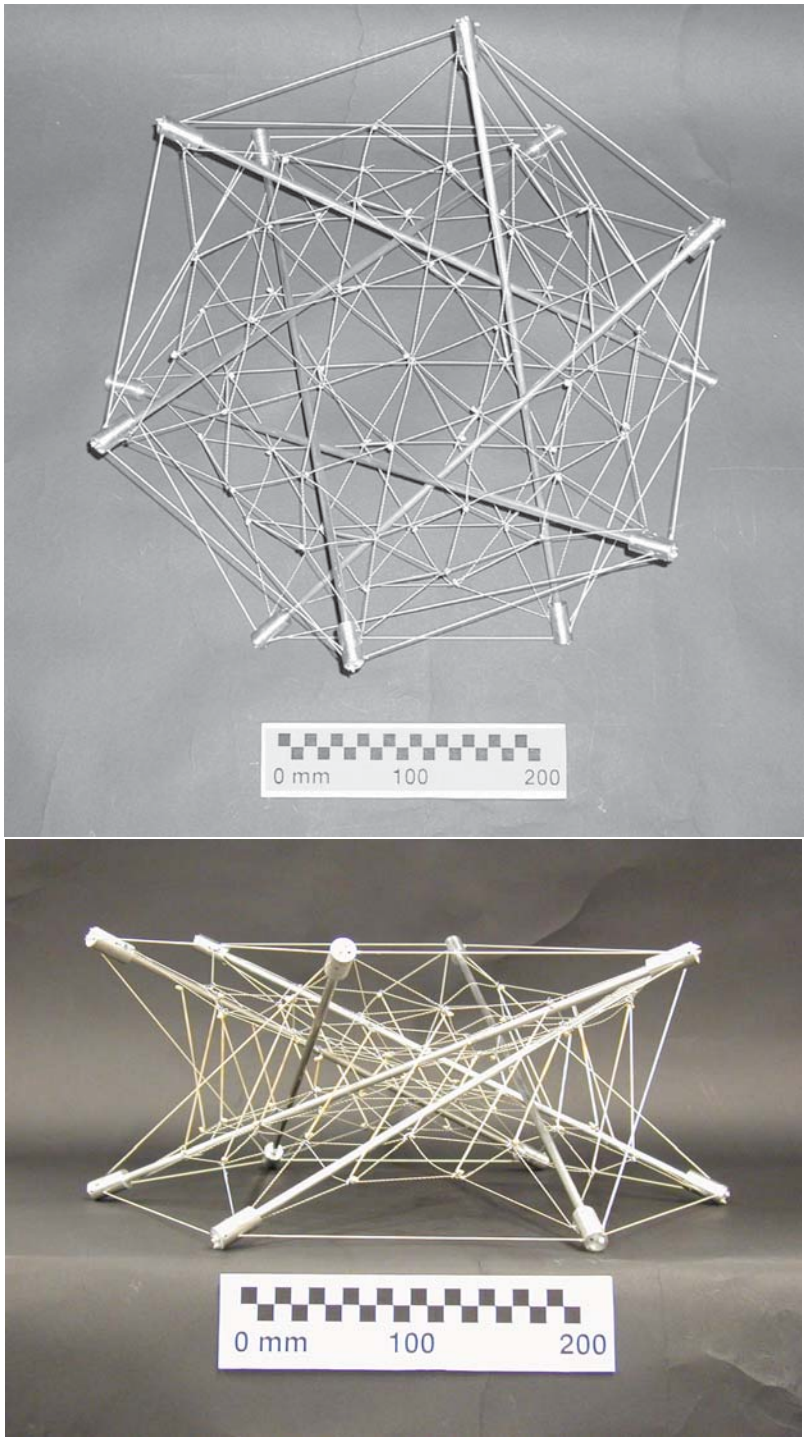

Figure 4.15: Model structure, expanded.

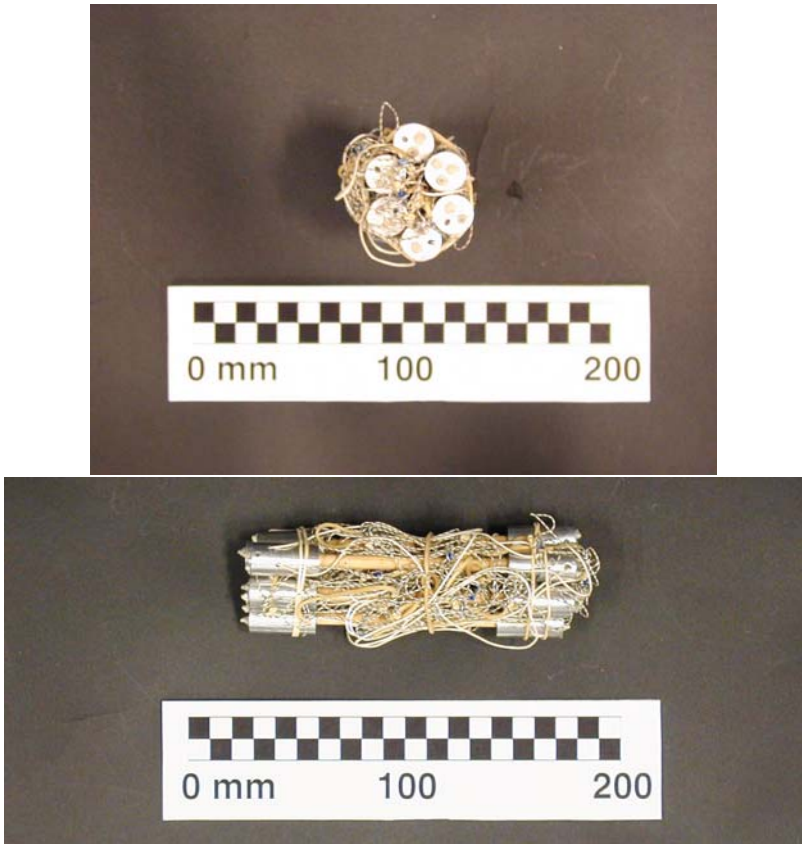

Figure 4.16: Model structure, folded.

4.5 Preliminary Design of 3 m Reflector

In this section we determine the main characteristics of a reflector to meet the DERA requirements ($D = 3$ m, $F = 1.2$ m, operation at ≈10 GHz). In particular, we aim to estimate the mass of the reflector.

4.5.1 Network Spacing

The surface error of the reflector will originate from a number of different sources, such as thermal distortion of the structure, etc. Only one contribution to the overall error budget can be considered at this stage, namely the effect of approximating the required paraboloid with a polyhedral surface. Therefore, it will be conservatively required that the root-mean-square error δ_{rms} should be less than about 1/100 of the wavelength.

At 10 GHz the wavelength is 30 mm and so the allowable error is 0.3 mm. For a spherical surface of radius R, Agrawal et al. (1981) have obtained the following relationship between δ_{rms} and the side length, L, of the triangles

$$\delta_{\text{rms}} = \frac{L^2}{8\sqrt{15}R} \tag{4.9}$$

For a shallow paraboloid the radius of curvature is approximately twice the focal length F, thus

$$R \approx 2F \tag{4.10}$$

For $D = 3.0$ m and $F = 0.4D = 1.2$ m Equation 4.9 can be solved for L and yields

$$L = 0.15 \text{ m}$$

Thus, the number of triangles across a 3 m diagonal of the hexagon will be 20, which means that there will be 10 rings of equilateral triangles. The corresponding total length of the cables that make up both nets is ≈ 300 m.

It is assumed that the members of the cable nets are made from graphite composite tapes (density 1740 kg/m^3) with a rectangular cross section of 5.0 mm by 0.2 mm. The weight of the joints in the net is accounted for by doubling the density of the tapes to 3480 kg/m^3. The total mass of the two nets is 1.04 kg.

4.5.2 Mesh

The reflective mesh is knitted gold-plated Molybdenum wire with a surface density of 0.025 kg/m^2. To account for seams and surface treatment this value is doubled to 0.05 kg/m^2.

Approximating the mesh area with the area of a spherical cap, we have

$$A = 2\pi RH$$

where R is the radius of the sphere, hence $R = 2F = 2.4$ m, and H is the height of the cap; hence $H = 0.469$ m. Thus, $A = 7.07$ m^2 and the corresponding mass is 0.35 kg.

4.5.3 Force in Springs

The tension in the mesh applies a lateral loading on the cable net to which it is attached, because the mesh forms a small kink, of angle L/R at the cross-over between adjacent triangles, see Figure 4.17(a). To prevent the sides of the triangles from becoming significantly distorted, the tension T in the cables of the net must be significantly larger than the transverse load.

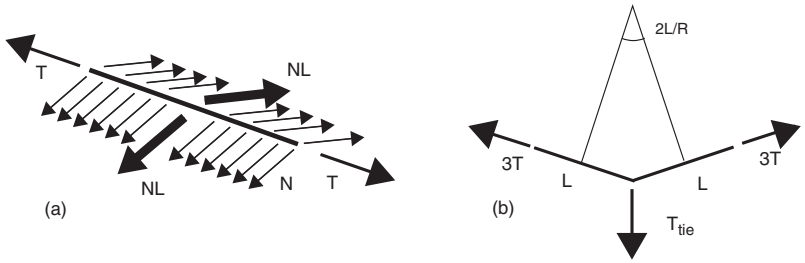

Figure 4.17: (a) Transverse load on cables and (b) equilibrium of a node.

For a preliminary estimate T will be set equal to ten times the mesh tension N multiplied by the triangle side length L. Taking $N = 2.0$ N/m the required tension in the net cables is $T = 3.0$ N. The force in the tension ties that is required to obtain the specified tension T in the cables is, see Figure 4.17(b) and recall that there are three cables through each node

$$T_{\text{tie}} = 3TL/R = 3 \times 3.0 \times 0.150/2.4 = 0.56 \text{ N} \tag{4.11}$$

It is interesting to note that the average pressure on the net, given by T_{tie} over the corresponding area of mesh[3] is 29 N/m^2. This pressure is considerably larger than the self-weight of the mesh under gravity, which is 0.5 N/m^2.

4.5.4 Ring Structure

The cable net analysed in Section 4.2 consisted of only three rings of triangles while the current one has ten rings. A preliminary estimate of the loads transmitted to the ring structure by the

[3]It is assumed that the surface associated with one node is twice the area of a triangle.

full-size net can be obtained by assuming that each cable in the three ring reflector represents 3.3 cables in a ten ring reflector. So, we can calculate the forces in the supporting structure by scaling the forces applied by the three ring net, which gives equivalent forces in the tension ties of 8 N. Table 4.1 lists the forces and length of the members of the ring structure.

Element	Force (N)	Length (m)
Horizontal cable	310	1.50
Lateral cable	376	1.96
Strut	−712	2.88

Table 4.1: Forces and lengths of elements of ring structure.

4.5.5 Design of Struts

The struts are designed to resist Euler buckling, subject to a minimum slenderness, L_e/r, of 200. Here, L_e is the effective length and r the radius of gyration. For a thin-walled tube of radius R

$$r = \sqrt{\frac{I}{A}} = \sqrt{\frac{\pi R^3 t}{2\pi R t}} = \frac{R}{\sqrt{2}}$$

Since $L_e = 2.88$ m, this yields $R > 0.0204$ m.

Graphite fibre tubes ($E = 227.5$ GN/m^2 and $\rho = 1740$ kg/m^3) with an outer diameter of 42 mm and wall thickness of 0.5 mm are selected and a check on the buckling load, 3.8 kN, is amply satisfied. The total length of these struts is 17.3 m and the total mass 1.96 kg.

4.5.6 Cable Dimensions

We assume that graphite fibre is the material used also for the cables of the ring structure. Its tensile strength is 2800 N/mm^2 and a design strength of 500 N/mm^2 is assumed. The maximum cable force is 1880 N. Thus, the required cross-sectional area is 3.76 mm^2 and, since the total length of the cables in the ring structure is 29.8 m, their mass is 0.19 kg.

4.5.7 Connections and Hinges

With a length of 2.88 m, each strut must be divided into four parts to fit into the STRV launch envelope, hence three self-locking hinges per strut are required.

It is planned to use the TSR hinges described in Section 3.2.1. It is conservatively assumed that the total mass of a hinge, including the attachments to the struts, is 0.2 kg. For the end connections between the strut and the ring structure cables a mass of 0.1 kg per strut is assumed.

Element	Quantity	Unit mass	Mass (kg)
Net cable	300 m	$8.7 \cdot 10^{-3}$ kg/m	1.04
Struts	17.3 m	0.113 kg/m	1.96
Ring cables	29.8 m	$6.6 \cdot 10^{-3}$ kg/m	0.19
Hinges	18	0.20 kg/item	3.60
End connections	12	0.050 kg/item	0.60
Mesh	7.07 m^2	0.050 kg/m^2	0.35
Total			7.74

Table 4.2: Mass estimates for 3 m diameter reflector.

4.6 Discussion and Conclusions

The proposed reflector concept offers a viable solution to the DERA requirements. Of course, a number of important aspects have yet to be considered, such as the attachment of the reflector to the spacecraft and the deployment sequence of the reflector.

Based on the estimates in Table 4.2 the total mass of a 3 m reflector with $F/D = 0.4$ is estimated at around 8 kg, which is considerably less than the mass budget initially allocated by DERA.

In concluding, it is noted that the proposed concept is—in principle—suitable also for offset configurations, although no detailed study has yet been done.

Appendix: Mesh Generation Procedure

In this appendix the procedure used for generating the triangular mesh of the paraboloidal cable nets is described in detail. The procedure is applicable to nets forming any regular polygon and is illustrated in Figure 4.18. First, an m-sided polygon is divided into m sectors, Figure 4.18(a). Each sector is then subdivided into $n \times n$ triangles and the edge nodes are projected onto parabolas with the required sag, Figure 4.18(b). Finally, the triangular mesh is projected onto the required paraboloidal surface giving the shape of the cable net, Figure 4.18(c).

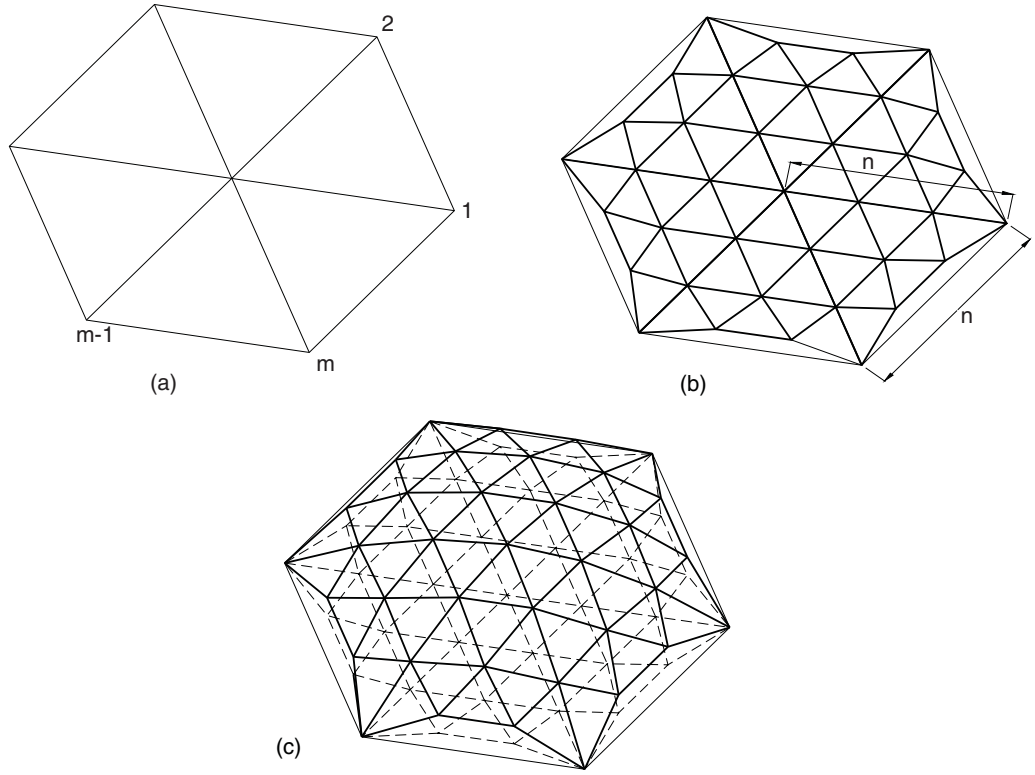

Figure 4.18: Generation of net; (a) m sided polygon; (b) subdivision of order n; (c) vertical mapping onto paraboloid.

In the final net the number of triangles t, elements b and joints j are respectively

$$t = mn^2 \tag{4.12}$$

$$b = m\frac{n(1+3n)}{2} \tag{4.13}$$

$$j = 1 + m\frac{n(1+n)}{2} \tag{4.14}$$

The subdivision of order n of a triangular sector is defined by the number of polygon sides,

m, the radius, R, and the two-dimensional sag-to-span ratio, ρ, defined as, Figure 4.19

$$\rho = \frac{\delta}{2R_0 \tan(\theta/2)} \tag{4.15}$$

where δ is the sag, $\theta = 2\pi/m$, and R_0 the "effective" radius of the net. Note that the span used in the definition, $2R_0 \tan(\theta/2)$, is different from the distance between the outer vertices which is $2R \tan(\theta/2)$.

Given the sag-to-span ratio, R_0 is calculated by subtracting from R the following lengths, Figure 4.19

$$\Delta_1 = R\frac{1 - \cos(\theta/2)}{\cos(\theta/2)} \tag{4.16}$$

$$\Delta_2 = \frac{\delta}{\cos(\theta/2)} \tag{4.17}$$

From Equations 4.15–4.17, the relation between R and R_0 is written as

$$\frac{R}{R_0} = \frac{1 + 2\rho \tan(\theta/2)}{\cos(\theta/2)} \tag{4.18}$$

The radius R is divided into n equal parts, corresponding to $n - 1$ rings of identical triangles. In the outer ring, the triangles are distorted by the sag of the edge cables. The edge joints are equidistantly positioned on an arc with radius r and opening angle γ, Figure 4.19

$$r = \frac{\delta^2 + R^2 \sin^2(\theta/2)}{2\delta} \tag{4.19}$$

$$\gamma = 2 \arccos \frac{r - \delta}{r} \tag{4.20}$$

The horizontal projection of the length of the edge elements is $2r \sin(\gamma/2n)$. It should also be noted that for odd values of n the actual two-dimensional sag of the edge elements will be slightly less than δ, as shown in Figure 4.19 for $n = 3$.

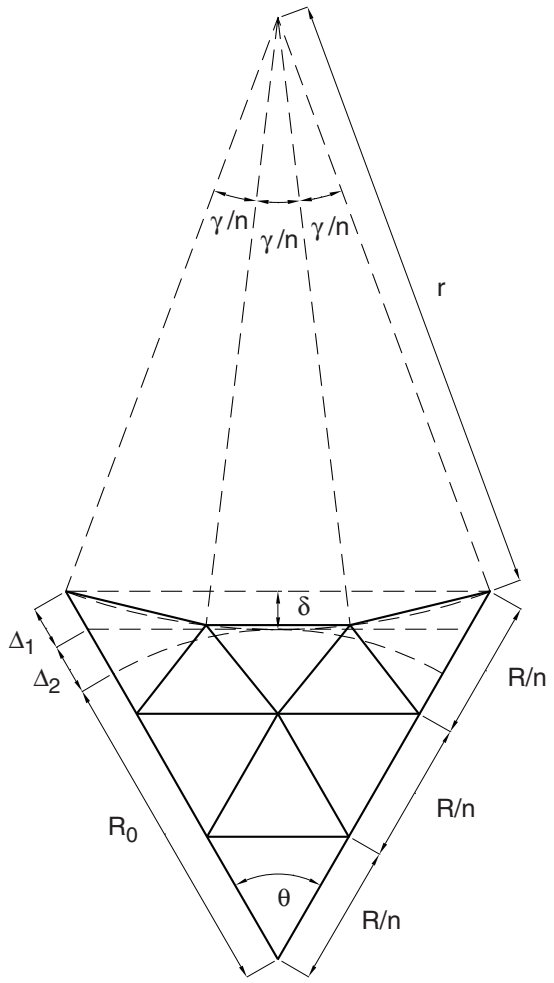

Figure 4.19: Triangular subdivision of a sector, here $n = 3$.

Chapter 5

SAR Structure

5.1 Background

The initial inspiration for the concept that will be presented came from a recent study in the Deployable Structures Laboratory. This study proposed a deployable SAR concept based on the JPL inflatable SAR (Lou et al. 1998) that is shown in Figure 5.1, but with the inflatable edge structure replaced with a foldable frame with TSR hinges.

It was envisaged that this frame will deploy and prestress a three-layer membrane with copper patches that provide the required radiation, ground and distribution planes of the SAR, as in the JPL inflatable SAR. Of course, the same structure could be used to support a single-layer membrane with printed antenna patches, as in the case of the DERA reflectarray.

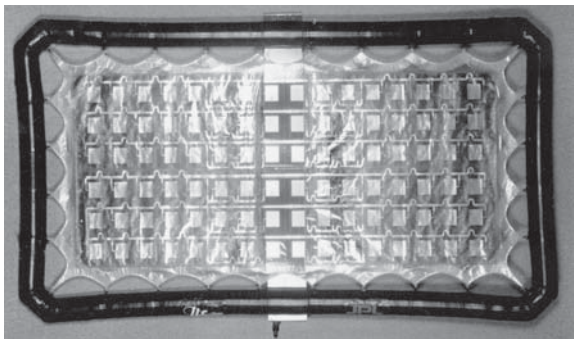

Figure 5.1: Small-scale model of JPL inflatable SAR (from Lou et al. 1998).

This previous concept is illustrated in Figure 5.2, which shows the deployment of a 1×2 m^2 (approximately) frame structure hanging vertically in the laboratory. This model includes a single membrane that is rolled up on a tube parallel to a short side of the frame, and is controlled by a DC motor.

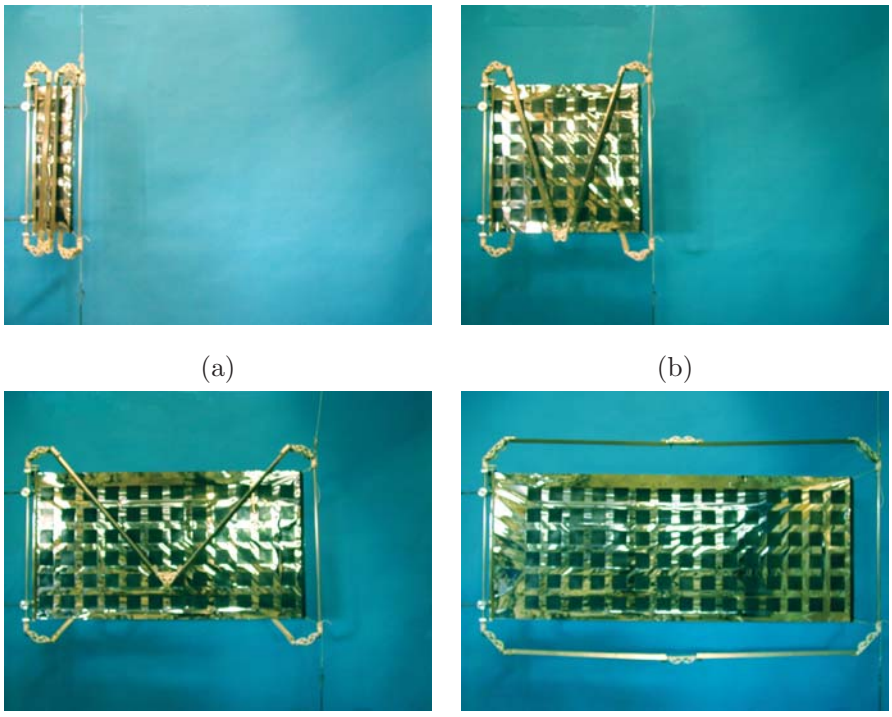

(a) (b)

(c) (d)

Figure 5.2: Deployment of rectangular frame supporting a single membrane.

A more detailed description of the concept of this foldable frame is given in Figure 5.3. It consists of six members of equal length, connected by revolute joints. In fact, the TSR hinges are not exactly revolutes, because the line of contact between the two rolling elements—which acts as an instantaneous axis of rotation—moves when the hinge rotates. This structure is not a mechanism, i.e. it would not be able to fold and deploy if all of its members were rigid and the hinges provided only a single degree of freedom. To permit folding, open section members have been used for the longer sides of the rectangle, to accommodate elastically—i.e. without any permanent deformation—the relative twisting between the ends of the members that occurs during folding.

The direction of the hinges is chosen such as to minimise the twist of the members while maintaining a sufficient degree of coupling between the members of the frame and also providing clearance for the membrane.

With reference to the fully deployed configuration shown in Figure 5.3, let us define as α the angle between the axes of the corner hinges and the normal to the plane of the frame, $\mathbf{n}$. This angle is defined to be positive if the vector aligned with the hinge axis and pointing in the same direction as $\mathbf{n}$ has an in-plane component that points towards the inside of the frame. The

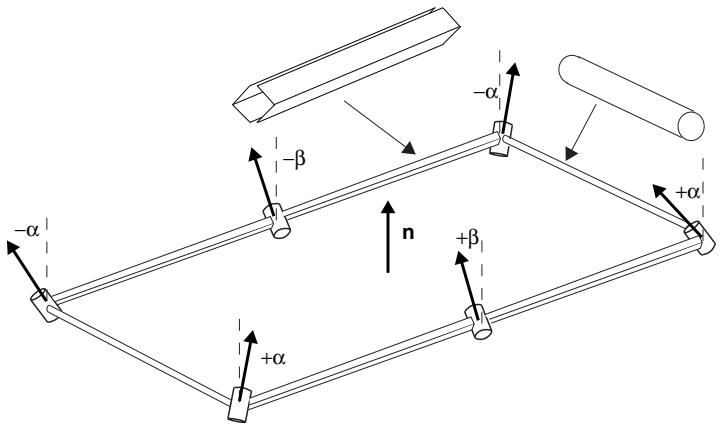

Figure 5.3: Schematic layout of deployable frame.

hinges in the middle of the longer sides form angles of $+\beta$ and $-\beta$ with $\mathbf{n}$, where the same sign convention applies.

Note that the in-plane projections of the axes of the corner hinges bisect the angles at the corners of the rectangle. Hence, it can be shown that α and β are related by

$$\tan\alpha = \sqrt{2}\tan\beta \tag{5.1}$$

If the short-side members of the frame are assumed not to deform, the long-side members are required to twist as the frame folds. The frame is normally designed such that its members have zero twist in the fully-deployed configuration. Hence, the maximum twist angle, in the fully-folded configuration, is β.

The frame of Figure 5.2 has $\beta \approx 15°$ and $\alpha = \arctan(\sqrt{2}\tan 15°) \approx 21°$. [1]

5.2 Proposed Concept

The approach proposed in Section 2.4 envisages three membranes rolled on three separate rollers that are attached to three interconnected deployable frames. Because there is no point in duplicating the members along the interface between adjacent frames, as it can only create interference problems, this concept is more accurately described as two rectangular frames connected by a "dummy" frame, see Figure 5.4. An additional mechanism is required to attach this structure to the side of the spacecraft; this attachment will not be discussed here.

[1] Note that if the corner hinges are perpendicular to the plane of the frame, $\alpha = 0°$, the frame becomes a mechanism and hence there is no twist.

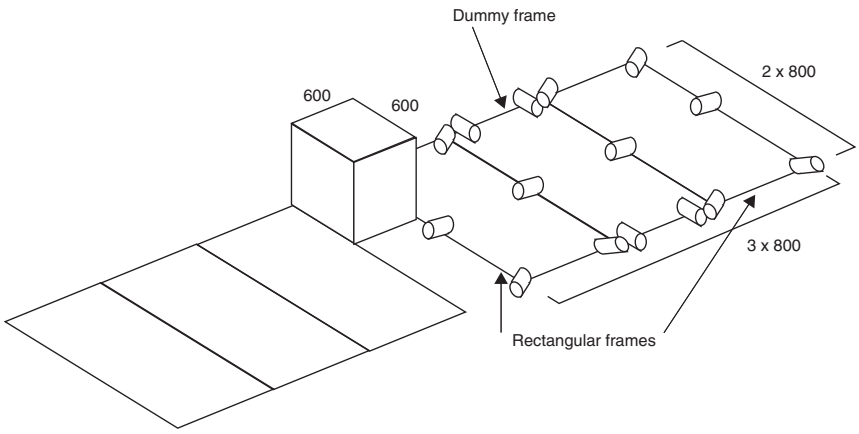

Figure 5.4: Proposed SAR concept, consisting of two rectangular frames connected by a "dummy" frame.

It was decided to construct a half-scale model to verify that the packaging scheme works as intended. A sketch of this structure is shown in Figure 5.5.

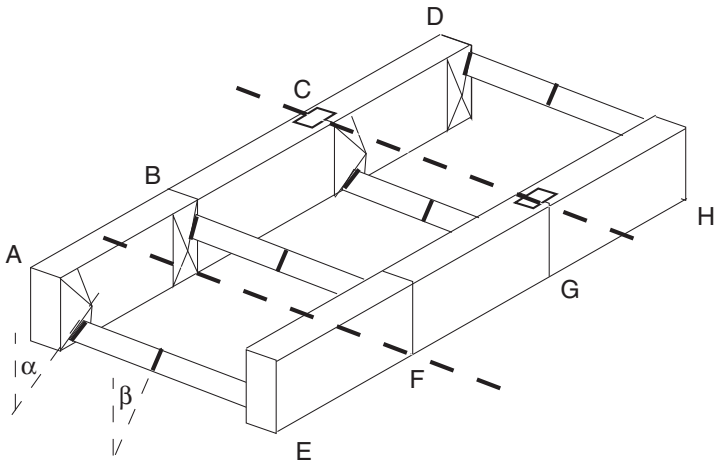

Figure 5.5: Layout of half-scale model.

The model consists of two longitudinal members, AD and EH, 1.2 m long and with cross-section of 60 mm × 30 mm, each divided into three parts of equal lengths that are connected by brass hinges located alternately on the lower and upper face of the members.

Four transverse Al-alloy angle members, with a brass hinge in the middle, link the longitudinal members. The connection between the transverse members and the longitudinal members is via brass hinges attached to timber wedges which are in turn glued to the longitudinal members. The hinge axes—starting from AE—are alternately $+\alpha$, $-\alpha$, etc. so that member AE

folds underneath the frame, BF above, etc.

Six free-turning Al-alloy tubes, held inside holes on the inner side of the timber wedges, support three 0.3×0.83 m^2 aluminised Mylar foils.

Figure 5.6(a) shows the model in the folded configuration; the bundle measures $0.15 \times 0.22 \times 0.45$ m^3, but note that only the length of this bundle is reasonably representative of a properly engineered structure; the other dimensions will depend on the cross-sectional dimensions of the members, hinges, and mechanisms that control the membrane. In Figures 5.6(b) and (c) the upper part, and then the lower part of the frame have been rotated through 180° respectively about CG and BF. In the remaining part of the sequence the longitudinal members, now straight, are pulled apart until the transverse become straight.

This model shows that the proposed concept is feasible and worth developing further.

5.3 Preliminary Analysis and Design Considerations

In order to determine preliminary dimensions for the full-size SAR frame a finite element model was made. In this model each longitudinal member consists of three 0.75 m long[2] CFRP tubes ($E = 100$ GN/m^2, $\rho = 1.5 \times 10^3$ kg/m^3) which, after some preliminary analyses, were chosen to have circular cross-section with 25 mm outside diameter and 2 mm thickness. Each transverse member consists of two 0.75 m long CFRP angle-section (25 mm wide and 1 mm thick, $I = 9.62 \times 10^{-9}$ m ^{4}). All of these members were modelled as beam elements, using Pro/Mechanica (Parametric Technology Corporation, 2000). The hinge angles were set, as for the structure of Figure 5.2, to $\beta = 15°$ and $\alpha = 21°$. Hence the maximum twist angle of a transverse member is 15°.

A check on the maximum shear stress in the angle sections was made. The shear modulus of CFRP can be estimated from

$$G = \frac{E}{2(1+\nu)} = 38 \text{ GPa} \tag{5.2}$$

having assumed the Poisson's ratio $\nu = 0.33$. The maximum shear stress in the angle section can then be found from (Timoshenko and Goodier, 1970)

$$\tau_{\max} = 2G\frac{t}{2}\phi \tag{5.3}$$

For $\phi = 15° \times \pi/(180 \times 0.75) = 0.35$ rad/m, Equation 5.3 gives a maximum shear stress of 13 N/mm^2. This is certainly acceptable.

[2] An additional length of 50 mm results from the half-length of the hinge.

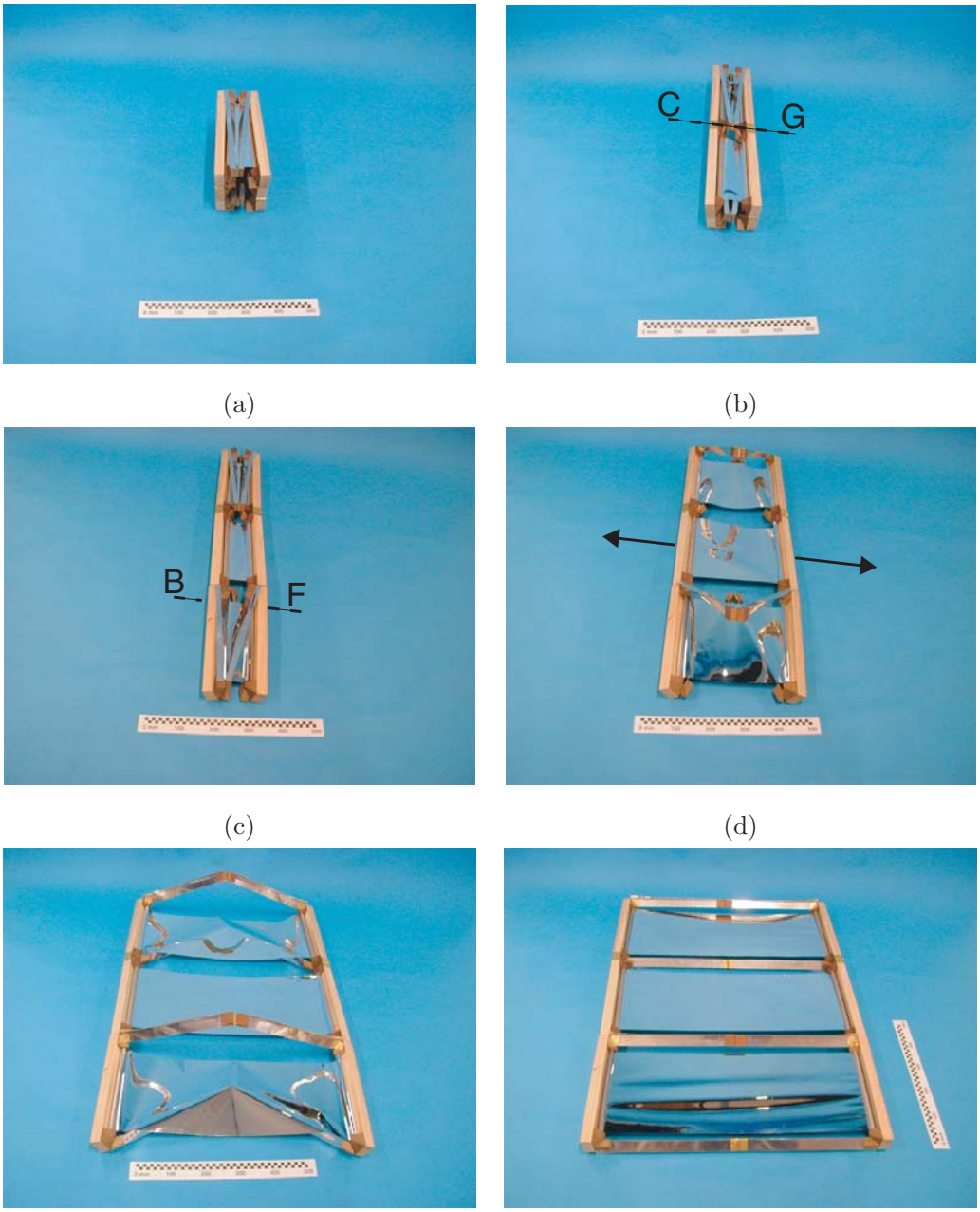

(a) (b)

(c) (d)

(e) (f)

Figure 5.6: Concept verification model.

The design of a lightweight deployable structure is primarily governed by stiffness requirements, as it is necessary that the fundamental natural frequency of vibration of the structure be sufficiently well separated from the rigid-body modes of the spacecraft. In this preliminary design it will be assumed that a fundamental natural frequency of around 1 Hz or above is required. The hinge properties have the same properties described in Section 3.2.1 and are modelled in the same way.

The boundary conditions are the same in all cases; the bottom-left corner of the frame plus the node in the middle of the bottom short edge are assumed to be fixed, i.e. attached to the spacecraft bus.

5.3.1 Frame with Four Transverse Members

The first design to be analysed was a frame with the layout of Figure 5.5, i.e. with four transverse members each with a hinge in the middle.

The mass of the membrane, with connectors and antenna patches, was taken to be 3 kg/m^2, as indicated in the DERA requirements report (Reynolds, 2000). The total surface area of the SAR is 2.4 m $\times$ 1.6 m = 3.84 m^2 and the corresponding mass is 11.5 kg[2]. It was simulated as 12 equal point masses of 0.96 kg attached at the ends of the members that form the longer edges of the frame.

The vibration properties of the frame, with the two different hinge models, were analysed with Pro/Mechanica and are shown in Figures 5.7 and 5.8. The corresponding natural frequencies are summarised in Table 5.1.

Mode	Stiff Hinges	TSR Hinges
1	0.99	0.80
2	2.00	1.30
3	2.62	1.82
4	4.45	3.48

Table 5.1: Natural frequencies (Hz) of frame with four transverse members.

The mode shapes are practically identical, but the stiff hinges give natural frequencies that are between 20% and 30% higher. These results give an indication of the frequency increase that can be achieved by re-designing the TSR hinges.

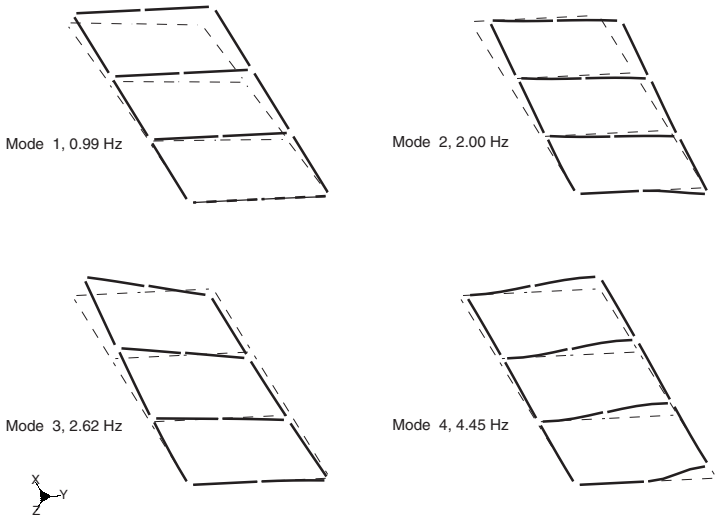

Figure 5.7: Mode shapes of frame with four transverse members (stiff hinges).

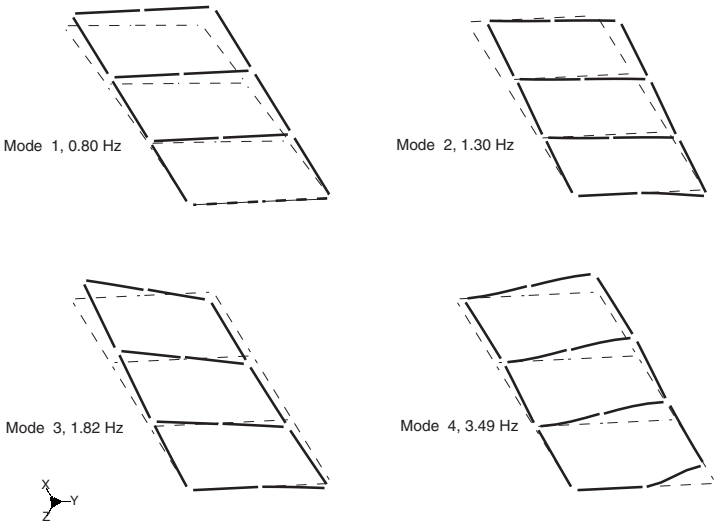

Figure 5.8: Mode shapes of frame with four transverse members (TSR hinges).

5.3.2 Frame with Two Transverse Members

An alternative design is obtained by removing the two intermediate transverse members. This change makes the frame lighter and simpler to design and manufacture. This modified frame was analysed again with the membrane simulated by 12 concentrated masses attached to the ends of the members forming the longer edges of the frame.

The results of this analysis are compared to those for the frame with the additional transverse members in Table 5.2 and the corresponding mode shapes can be seen in Figure 5.9. It can be seen that removing two of the transverse members has the effect of increasing the natural frequency of the frame, because the effect of lowering the mass of the frame is greater than the associated stiffness reduction.

Mode	4 transverse members	2 transverse members
1	0.80	1.01
2	1.30	1.30
3	1.80	1.92
4	3.48	3.84

Table 5.2: Natural frequencies (Hz) of frames with different numbers of transverse members, joined by TSR hinges.

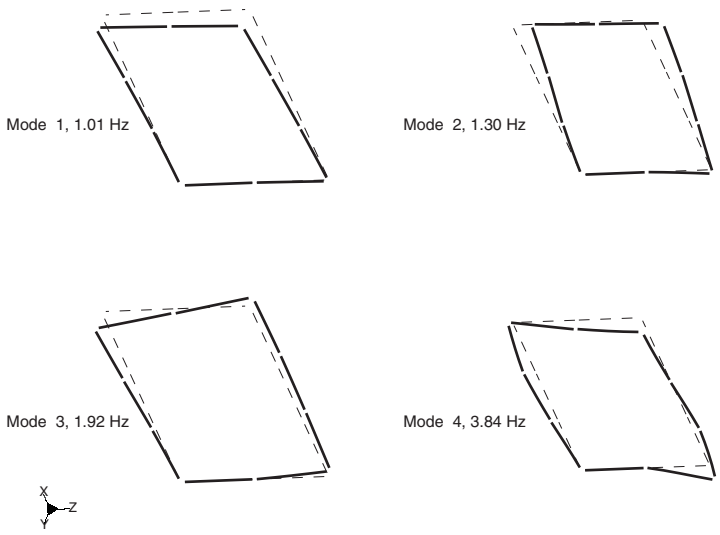

Figure 5.9: Modes of frame with two transverse members (TSR hinges).

5.4 Selected Scheme

There is one major problem with the design considered in Section 5.3.2 in that the pre-tension in the membrane, needed to keep the membrane taut and dynamically stable, is applied to an unsupported length of the frame.

The value of the required prestress in the membrane can be estimated from the requirement that the fundamental frequency of vibration should be above 1 Hz. A preliminary estimate of this frequency can be obtained by considering a cable of length ℓ, mass per unit length m and subject to prestress T_0. Here

$$f = \frac{1}{2\ell}\sqrt{\frac{T_0}{m}} \tag{5.4}$$

This expression can be re-arranged to find

$$T_0 \geq 4f^2\ell^2 m \tag{5.5}$$

Considering a 1 m width of membrane, and substituting $\ell = 1.6$ m, $f = 1$ Hz, and $m = 3$ kg/m we obtain

$$T_0 \geq 30.7 \text{ N}$$

Hence, we will assume that the *transverse prestress* is 100 N/m.

The bending deflection of a 3 m long tube with the cross-sectional properties described in Section 5.3 and subjected to a distributed loading of 100 N/m is about 30 mm. This is clearly unacceptable.

Two possible solutions to this problem are to either increase the bending stiffness of the longitudinal members by at least an order of magnitude, which would also increase the mass of the frame, or to replace the three separate membranes with a single membrane that is connected to the frame only at the corners. This second approach was selected, as it is also advantageous in terms of the overall planarity and continuity of the membrane.

A uniformly distributed edge load can be applied to a membrane by means of an edge cable with parabolic shape. The tension in this cable is dependent on the span, ℓ, the dip, d, and the distributed load per unit length, w. The end reactions have vertical component $V = w\ell/2$ and the horizontal component is

$$H = \frac{w\ell^2}{8d} \tag{5.6}$$

In the present case a value of $\ell = 2.4$ m and a non-dimensional dip of $d/\ell = 0.05$ are assumed. Using a shallower cable may be desirable, to increase the area of the membrane, but

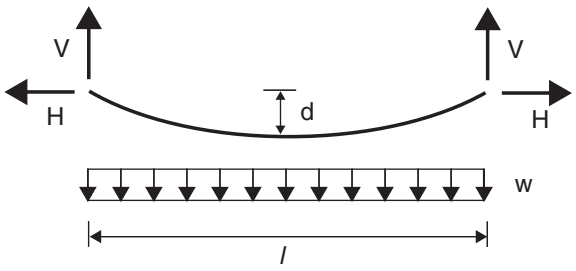

Figure 5.10: Equilibrium of edge cable.

would further increase H, thus increasing the compression in the members of the frame. It is also likely to result in significant elastic stretching of the cable, which would then need to be accounted for in the analysis.

Since the required prestress in the membrane is 100 N/m, $H = 600$ N and $V = 120$ N. The force components V and H are equilibrated by equal and opposite corner forces at the corners of the frame, Figure 5.11, hence the longitudinal members have to resist a compressive force equal to H and the transverse members a compressive force of V.

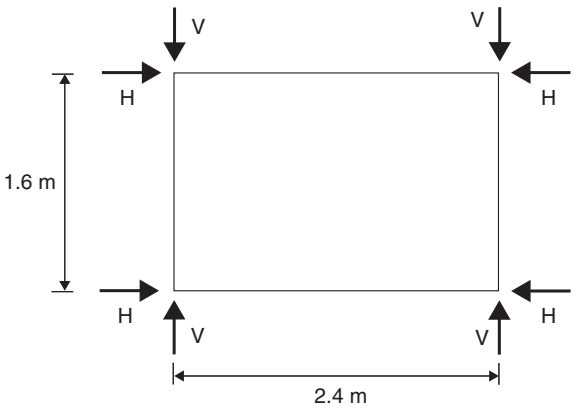

Figure 5.11: Corner forces on frame structure.

These loads were compared to the following, preliminary estimates of the buckling loads for the members of the frame. Assuming each member to be effectively pin-jointed at the ends, i.e. neglecting the bending stiffness of the joints of the frame, the Euler buckling formula is

$$P = \frac{\pi^2 EI}{\ell^2} \tag{5.7}$$

The longitudinal members have $\ell = 2.4$ m, $E = 100$ GN/m^2, and $I = 9.6282 \times 10^{-9}$ m^4. Equation 5.7 then gives a buckling load of 1650 N, which is well above the compressive force of

600 N that is applied.

The transverse members have $\ell = 1.6$ m, $E = 100$ GN/m^2 as before, and $I_{\min} = 1.30 \times 10^{-9}$. A similar calculation gives a buckling load of 502 N, again well above the 120 N compressive force applied by the membrane.

The use of edge cables such as those proposed above will reduce the effective area that can be used as a SAR surface. For example, the chosen dip $d/\ell = 0.05$ reduces the effective area to 90% of the area enclosed by the rectangular frame. However, the area lost can be regained by continuing the surface over and beyond the edge cable and holding this part of the membrane under light tension. It is important to keep this tension small, to prevent excessive deflection, and the effect of this deflection of the longitudinal members of the frame in reducing the buckling load should also be considered.

The use of a single membrane requires a single roller on which to wrap the membrane, instead of the three separate rollers used in the solution shown in Figure 5.6. Clearly, the roller and membrane rolled over it need to be folded in a way that is compatible with the frame. This can be achieved by using tape-spring hinges that join three tubular elements to form a continuous roller. In order to avoid crumpling the membrane after it has been rolled around the roller, it is suggested that a series of parallel cuts could be made in the membrane, as shown in Figure 5.12. When the membrane is rolled up these cuts become aligned and so the membrane is continuous only above the tape springs.

A detailed design and a rendering of the frame with membrane, produced with Pro/Engineer, can be seen in Figure 5.12. Note that the edge cable is terminated as close as possible to the corners of the frames, to minimise the bending moments in the frame.

5.4.1 Mass Estimate

Table 5.3 shows a breakdown of the estimated mass of a 2.4 $\times$ 1.6 m^2 SAR structure with the design outlined in Figure 5.12, but without considering the connection between the SAR and the spacecraft bus.

The members of the frame are all made from CFRP. The density of the membrane, including antenna patches and connectors, has been assumed to be 3 kg/m^2; the mass of the redundant motors that restrain and tension the membrane, including attachments is estimated at 0.4 kg each. The total mass of the SAR is thus 15.5 kg and the mass of a complete, 5 m long SAR is around 31 kg, plus primary deployment mechanisms.

It is envisioned that in a final design the cross-section of the beam elements of the frame

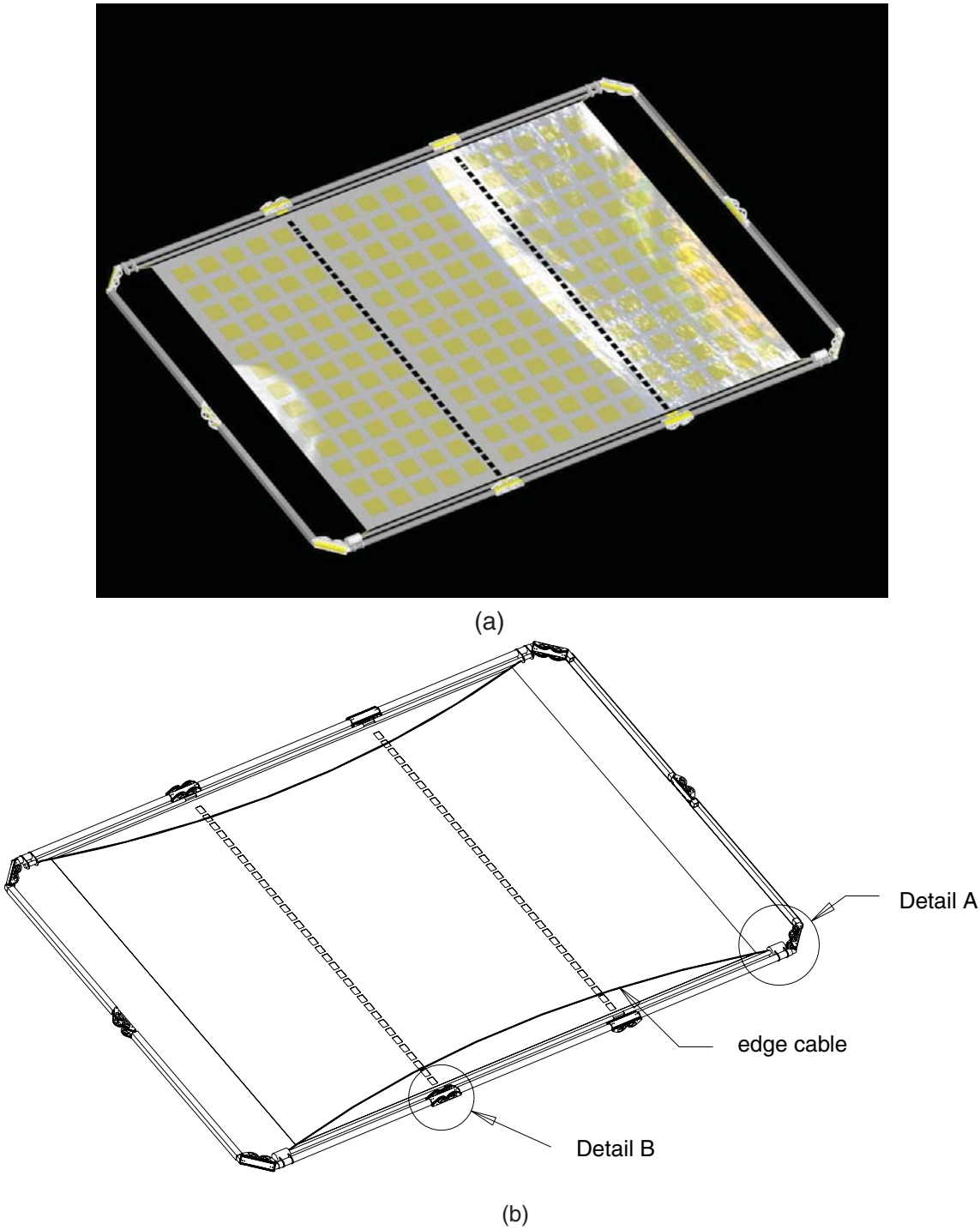

Figure 5.12: Detailed design of frame with two transverse members, supporting a single membrane.

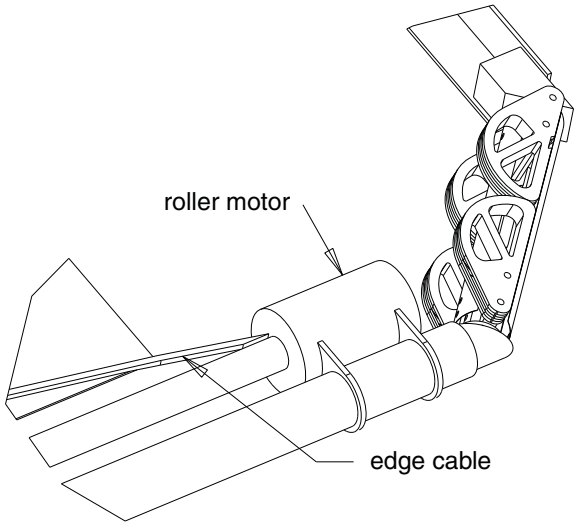

Figure 5.13: Detail A.

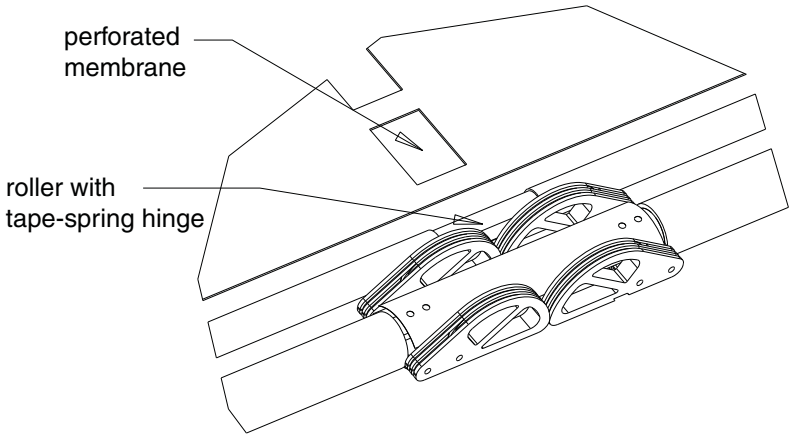

Figure 5.14: Detail B.

may well increase, however as these account for only 1.3 kg of the total mass of the structure, such a modification would have only a fairly small impact on the overall mass.

Element	Quantity	Unit Mass	Mass (kg)
Membrane	3.84 m^2	3 kg/m^2	11.52
Hinges	10	0.15 kg	1.5
Angle Beams	4	0.1 kg	0.4
Round tube beams	6	0.15 kg	0.9
Membrane rollers	2	0.19 kg	0.38
Motors	2	0.4 kg	0.8
Total			15.5

Table 5.3: Mass breakdown for 2.4 $\times$ 1.6 m^2 SAR structure (kg).

5.4.2 Finite-Element Analysis

A simple finite element model of this frame was set up in Pro/Mechanica with the mass of the membrane modelled as four point masses of 2.88 kg each. The mode shapes can be seen in Figure 3.5. The results of this analysis are compared in Table 5.4 to those for the frame with three separate membrane panels, considered in Section 5.3.2. It can be seen that the first three natural frequencies are lower if a single membrane is used; this is because a greater part of the mass of the membrane has been concentrated at the end of the frame that is further away from the spacecraft.

Mode	Single membrane	Membrane in 3 pieces
1	0.83	1.01
2	1.16	1.30
3	1.77	1.92
4	3.89	3.84

Table 5.4: Natural frequencies (Hz) of frames with two transverse members.

A more refined ABAQUS (Hibbit et al., 1999) finite-element model of the same structure was set up, to investigate in greater detail the vibration behaviour of the prestressed membrane. The frame was assumed to be a rigidly-jointed rectangle with base length of 2.4 m and height of 1.6 m, fixed to the spacecraft half way along one of the shorter edges of the rectangle. The members of the frame have the same properties as in Section 5.3.2.

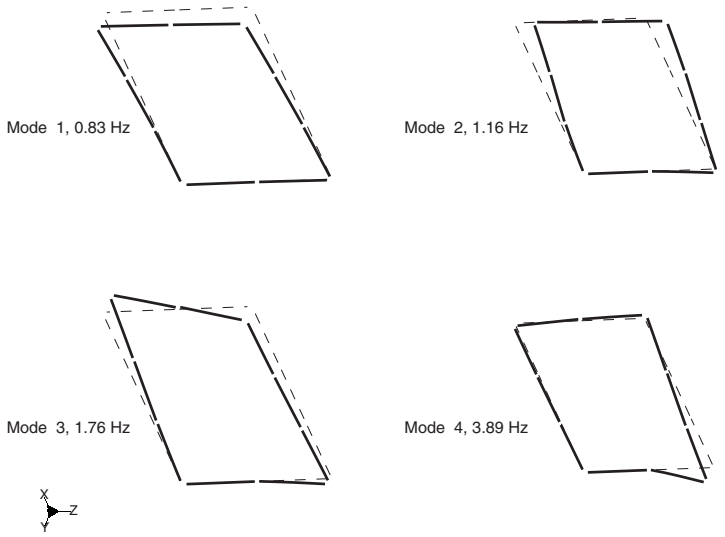

Figure 5.15: Mode shapes of frame with two transverse members (TSR hinges) and a single membrane.

The membrane is 0.125 mm thick Kevlar-reinforced Kapton foil whose equivalent density is defined such that a mass of 3 kg/m^2 is obtained. The edge cords have a cross-sectional area of 2 mm^2 and are made of Kevlar. The properties of these materials are given in Table 5.5. The prestress in the membrane was assumed to be $w = 100$ N/m, as discussed earlier, in the transverse direction.

Parameter	Membrane	Cable	Frame
Density (kg/m^3)	24000	1450	1500
Young's Modulus (GPa)	11.9	131	100
Poisson's Ratio	0.3	0.3	0.3

Table 5.5: Properties of membrane and frame members.

The membrane was modelled using 4 node quadrilateral elements M3D4. These elements are surface elements that transmit in-plane forces only (no moments) and have no bending stiffness. This means that it is necessary to prestress them before any vibration analysis is carried out. The frame was modelled with Euler-Bernoulli B33 beam elements. The parabolic edge cables were modelled with T3D2 elements.

The most complex part of the analysis is the application of the state of prestress to the membrane, with corresponding stresses in the edge cables and the frame supporting them. Kukathasan (2000) has recently carried out an extensive study of how this can be done with the ABAQUS package.

In the present case, this was done by applying an initial stress of 300 N/mm^2 to the edge cables, using the **INITIAL CONDITIONS, TYPE=STRESS* option, before applying any of the **STEP* options. To account for the geometric stiffness induced by the prestress, the following non-linear calculation procedures were used.

To avoid convergence problems, the ABAQUS analysis was divided into the following four steps.

- Step 1. All nodes of the cable elements are held fully constrained while an initial, non-linear equilibrium analysis is carried out. The elements that make up the frame are subject to their normal boundary conditions. In this step there is no stress transfer from the cable elements to the membrane.

- Step 2. Most of the constraints applied to the cables are released, only the ends of the cables are held fully constrained. Again, a non-linear equilibrium iteration is carried out, which has the effect of transferring some of the stress in the cables to the membrane. The transverse stress in the membrane increases to a fairly uniform 8×10^5 N/m^2, corresponding to 100 N/m, Figure 5.16(a). The longitudinal stress in the membrane is at least an order of magnitude lower than the transverse stress. The members of the frame remain unstressed.

- Step 3. The constraints at the ends of the edge cables are released and a further non-linear iteration is carried out, with the structure subjected only to its actual boundary conditions. However, a considerable compressive stress, see Figure 5.17, builds up in the membrane, in the longitudinal direction, due to the shortening of the edge members of the frame.

  To avoid these compressive stresses, unidirectional constraints are applied to the vertical edges of the membrane and the step is repeated. This has the effect of imposing longitudinal stresses of up to one third of the transverse stresses.[3] The resulting stress distribution is shown in Figure 5.18.

- Step 4. The boundary conditions are, again, changed to the actual ones by using **BOUNDARY, OP=NEW* option and a linear frequency extraction step is carried out.

Two solution methods are available in ABAQUS: the subspace iteration method and the Lanczos method. The Lanczos eigensolver is faster and more effective for models with many

[3] In practice, it is likely that edge cables will be required also along the short edges of the membrane, to apply a small amount of longitudinal prestress.

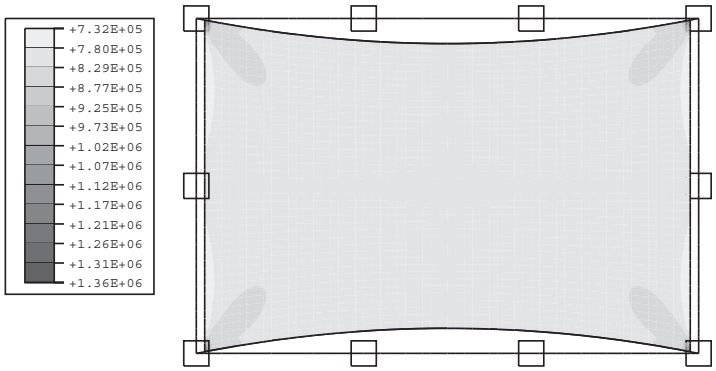

(a) Transverse

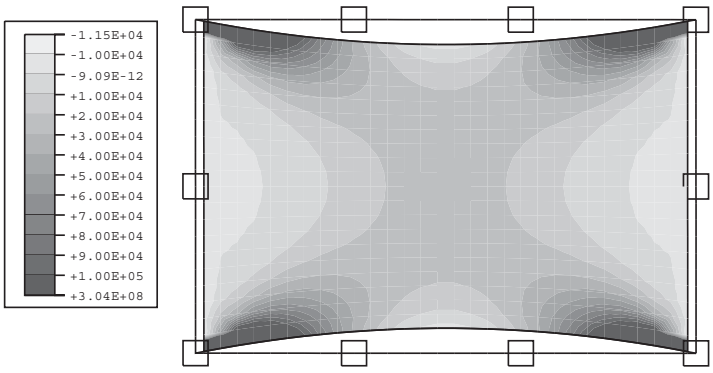

(b) Longitudinal

Figure 5.16: Stress field after step 2 ($\mathrm{N/m^2}$).

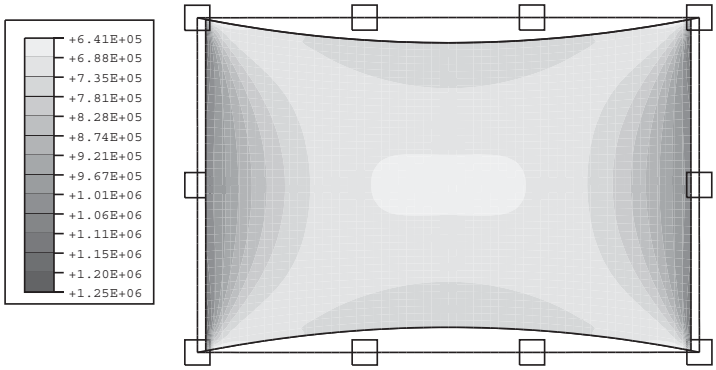

(a) Transverse

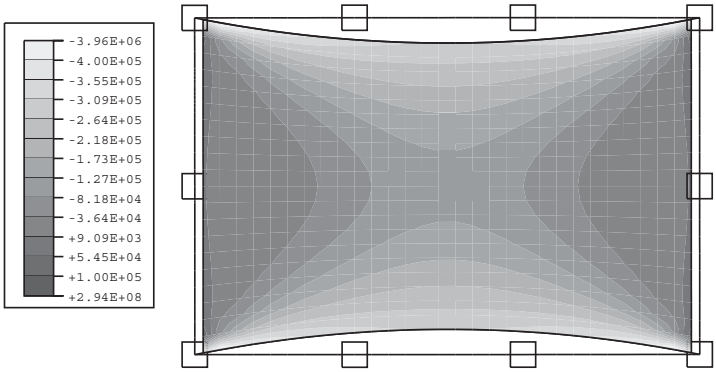

(b) Longitudinal

Figure 5.17: Stress field after initial step 3 (N/m^2).

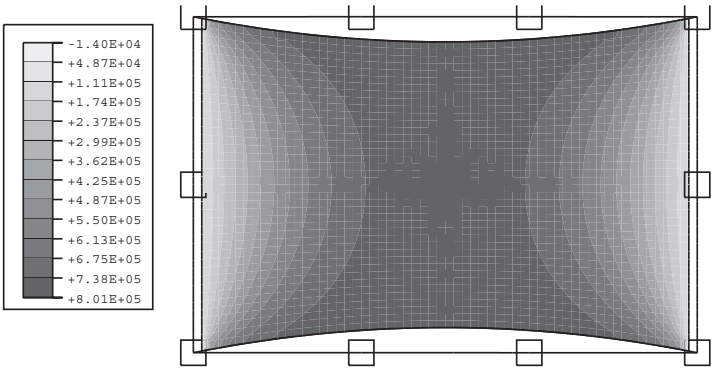

(a) Transverse

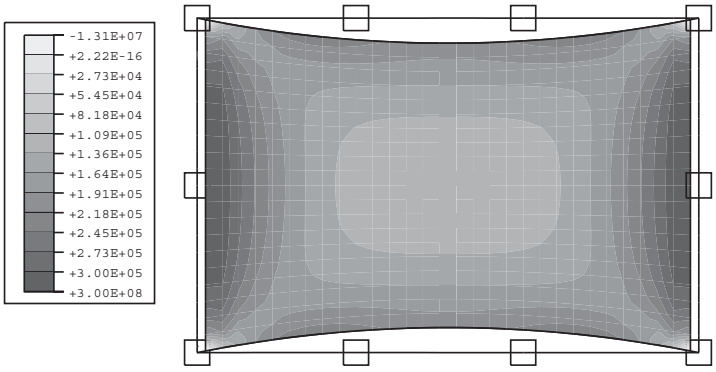

(b) Longitudinal

Figure 5.18: Stress field after step 3 ($\mathrm{N/m^2}$).

degrees of freedom and therefore it was chosen.

Figure 5.19 shows the first eight mode shapes of this structure. Note that the fundamental frequency is higher (0.93 Hz) than in the lumped-mass model (0.83 Hz); the likely reason is that the current model has stiff hinges. The in-plane stiffness of the membrane has the effect of suppressing mode 2, i.e. the "shear" mode, obtained from the earlier analysis. The actual mode 2 (1.58 Hz) involves only the membrane, and hence can be compared to the prestressed cable mode of Equation 5.4. Mode 3 involves the membrane, again, coupled with bending of the frame. Among the higher modes, note that in mode 5 the frame twists about its axis; it is analogous to mode 3 predicted by the simple model.

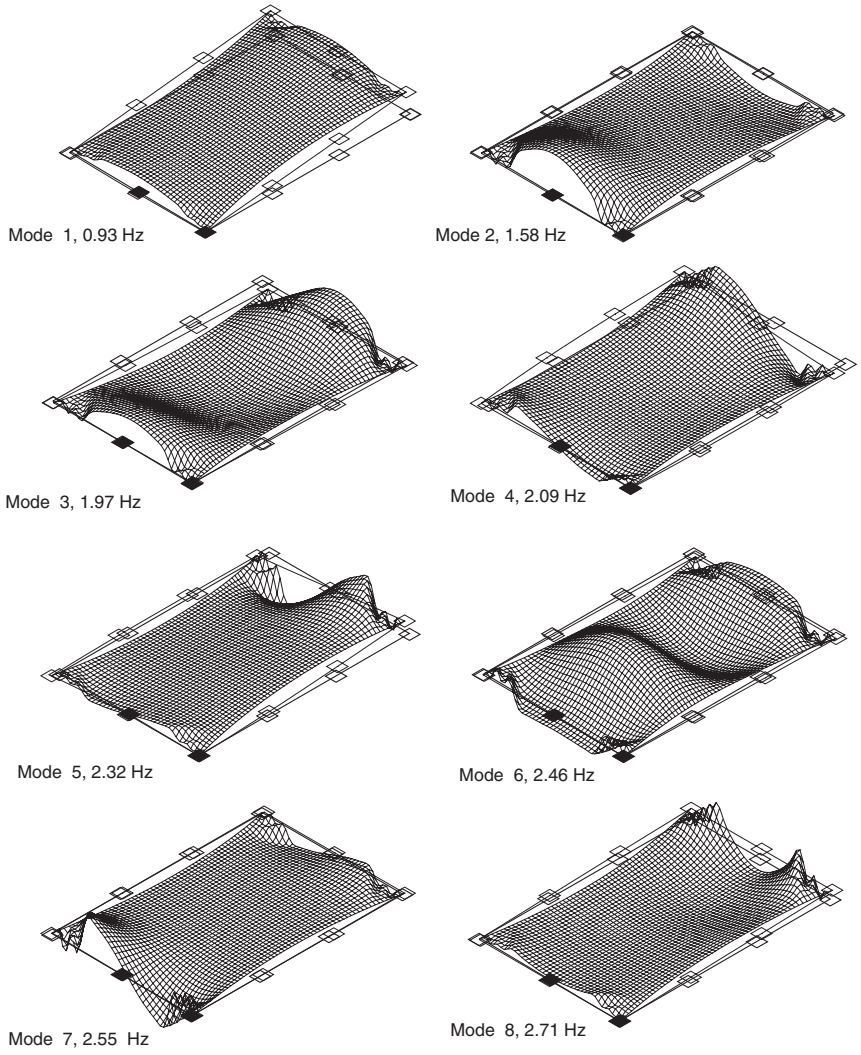

Figure 5.19: First 8 mode shapes and corresponding natural frequencies of frame with two transverse members, supporting a single membrane. Outline of undeformed edge frame shown for reference.

5.5 Discussion

The feasibility of the 2.4×1.6 m^2 deployable SAR concept envisaged in Section 2.4 has been explored. It has been shown that it is, indeed, feasible and a preliminary design of a CFRP structure with TSR self-locking hinges has been presented. The proposed structure has a fundamental natural frequency of around 0.9 Hz, will package into a volume of $0.15 \times 0.22 \times 0.8$ m^3, and has a mass of around 15.5 kg.

A number of issues related to the proposed design remain open at this stage. Most importantly, the folding arrangement of the membrane needs to be investigated further, particularly the effect of the perforations along the part of the membrane that is rolled around the hinges in the roller element. There may be effects on the structural integrity and planarity of the membrane, after it is deployed, which need to be investigated.

Another issue that needs to be further examined is how the frame would be deployed. It is envisaged that the whole structure would be deployed by the strain energy stored in the springs. The longitudinal members would be deployed first, by releasing a clamping band around the whole bundle, while the membrane rollers are kept locked. This would be followed by the transverse deployment of the frame, controlled by the rate of turning of the rollers.

References

Agrawal, P. K., Anderson, M. S. and Card, M. F. (1981). Preliminary design of large reflectors with flat facets. *IEEE Transactions on Antenna and Propagation*, AP-29, 688-694.

Calladine, C. R. (1978). Buckminster Fuller's Tensegrity structures and Clerk Maxwell's rules for the construction of stiff frames. *International Journal of Solids and Structures*, **14**, 161-172.

Hibbit, Karlsson and Sorensen (1999). *ABAQUS Version 5.8.1.* Pawtucket, RI 02860.

Iqbal, K. and Pellegrino, S. (2000). Bi-stable composite shells. In: *Proc. 41st AIAA/ASME/ ASCE/AHS/ASC Structures, Structural Dynamics and Materials Conference*, 3-6 April 2000, Atlanta GA, AIAA 2000-1385.

Kukathasan, S. (2000). *Vibration of prestressed membrane structures.* M.Phil. Dissertation, University of Cambridge.

Lou, M. C., Feria, V. A. and Huang, J. (1998). Development of an inflatable space synthetic aperture radar. In: *Proc. 39th AIAA/ASME/ ASCE/AHS/ASC Structures, Structural Dynamics and Materials Conference*, 20-23 April 1998, Long Beach, California pp 2783-2788.

Miura, K. (1986). Concept of tension activated cable lattice antenna. In: *Proc. 37th IAF Congress*, 4-11 October, Innsbruck, Austria, IAF-86-206.

Miura, K. and Miyazaki, Y. (1990). Concept of the tension truss antenna. *AIAA Journal*, **28**, 1098-1104.

Pak, H. Y. E. (2000). *Deployable Tensegrity structures.* M.Eng. Project Report, Department of Engineering, University of Cambridge.

Parametric Technology Corporation (2000). *Pro/Engineer, Pro/Mechanica Version 2000i2.* Walton, MA 02453.

Pellegrino, S. (1993). Structural computations with the Singular Value Decomposition of the equilibrium matrix. *Int. J. Solids Structures*, **30**, 3025-3035.

Pellegrino, S., Green, C., Guest, S. D. and Watt, A. M. (1999). *SAR Advanced Deployable Structures*. Report to MMS Space Systems UK.

Reynolds, T. (2000). *Small satellite deployment mechanisms requirement report*. DERA Report DERA/KIS/SPACE/CR000495/1.0.

Thomson, M. W. (1997). The AstroMesh deployable reflector. In: *Proc. Fifth International Mobile Satellite Conference (IMSC'97)*, 16-18 June 1997, Pasadena, CA pp 393-398. JPL Publication 97-11.

Timoshenko, S. P. and Goodier, J. N. (1970). *Theory of Elasticity*, Third edition. McGraw-Hill, Tokyo.

Watt, A. M. (2000). *Lightweight deployable SAR structures*. M.Phil. Dissertation, University of Cambridge.